

# MedShapeNet - A Large-Scale Dataset of 3D Medical Shapes for Computer Vision

Jianning Li, Antonio Pepe, Christina Gsaxner, Gijs Luijten, Yuan Jin, Narmada Ambigapathy, Enrico Nasca, Naida Solak, Gian Marco Melito, Afaque R. Memon, Xiaojun Chen, Jan Stefan Kirschke, Ezequiel de la Rosa, Patrick Ferdinand Christ, Hongwei Bran Li, David G. Ellis, Michele R. Aizenberg, Sergios Gatidis, Thomas Küstner, Nadya Shusharina, Nicholas Heller, Vincent Andrearczyk, Adrien Depeursinge, Mathieu Hatt, Anjany Sekuboyina, Maximilian Löffler, Hans Liebl, Reuben Dorent, Tom Vercauteren, Jonathan Shapey, Aaron Kujawa, Stefan Cornelissen, Patrick Langenhuizen, Achraf Ben-Hamadou, Ahmed Rekik, Sergi Pujades, Edmond Boyer, Federico Bolelli, Costantino Grana, Luca Lumetti, Hamidreza Salehi, Jun Ma, Yao Zhang, Ramtin Gharleghi, Susann Beier, Arcot Sowmya, Eduardo A. Garza-Villarreal, Thania Balducci, Diego Angeles-Valdez, Roberto Souza, Leticia Rittner, Richard Frayne, Yuanfeng Ji, Soumick Chatterjee, Andreas Nürnberger, João Pedrosa, Carlos Ferreira, Guilherme Aresta, António Cunha, Aurélio Campilho, Yannick Suter, Jose Garcia, Alain Lalande, Emmanuel Audenaert, Claudia Krebs, Timo Van Leeuwen, Evie Vereecke, Rainer Röhrig, Frank Hölzle, Vahid Badeli, Kathrin Krieger, Matthias Gunzer, Jianxu Chen, Amin Dada, Miriam Balzer, Jana Fragemann, Frederic Jonske, Moritz Remppe, Stanislav Malorodov, Fin H. Bahnsen, Constantin Seibold, Alexander Jaus, Ana Sofia Santos, Mariana Lindo, André Ferreira, Victor Alves, Michael Kamp, Amr Abourayya, Felix Nensa, Fabian Hörst, Alexander Brehmer, Lukas Heine, Lars E. Podleska, Matthias A. Fink, Julius Keyl, Konstantinos Tserpes, Moon-Sung Kim, Shireen Elhabian, Hans Lamecker, Dženan Zukić, Beatriz Paniagua, Christian Wachinger, Martin Urschler, Luc Duong, Jakob Wasserthal, Peter F. Hoyer, Oliver Basu, Thomas Maal, Max J. H. Witjes, Ping Luo, Bjoern Menze, Mauricio Reyes, Christos Davatzikos, Behrus Puladi, Jens Kleesiek, Jan Egger

**Abstract**—We present *MedShapeNet*, a large collection of anatomical shapes (e.g., bones, organs, vessels) and 3D surgical instrument models. Prior to the deep learning era, the broad application of statistical shape models (SSMs) in medical image analysis is evidence that *shapes* have been commonly used to describe medical data. Nowadays, however, state-of-the-art (SOTA) deep learning algorithms in medical imaging are predominantly voxel-based. In computer vision, on the contrary, *shapes* (including, voxel occupancy grids, meshes, point clouds and implicit surface models) are preferred data representations in 3D, as seen from the numerous shape-related publications in premier vision conferences, such as *the IEEE/CVF Conference on Computer Vision and Pattern Recognition (CVPR)*, as well as the increasing popularity of *ShapeNet* (about 51,300 models) and *Princeton ModelNet* (127,915 models) in computer vision research. *MedShapeNet* is created as an alternative to these commonly used shape benchmarks to facilitate the translation of data-driven vision algorithms to medical applications, and it extends the opportunities to adapt SOTA vision algorithms to solve critical medical problems. Besides, the majority of the medical shapes in *MedShapeNet* are modeled directly on the imaging data of real patients, and therefore it complements well existing shape benchmarks comprising of computer-aided design (CAD) models. *MedShapeNet* currently includes more than 100,000 medical shapes, and provides annotations in the form of paired data. It is therefore also a freely available repository of 3D models for extended reality (virtual reality - VR, augmented reality - AR, mixed reality - MR) and medical 3D printing. This white paper describes in detail the motivations behind *MedShapeNet*, the shape acquisition procedures, the use cases, as well as the usage of the online shape search portal: <https://medshapenet.ikim.nrw/>.

**Index Terms**—3D Medical Shapes, ShapeNet, Benchmark, Anatomy Education, Shapeomics, Deep learning, Augmented Reality, Virtual Reality, Mixed Reality, 3D Printing, Stereolithography, Face Reconstruction, Medical Data Sharing, Data Privacy



- J. Li, G. Luijten, N. Ambigapathy, E. Nasca, A. Dada, M. Balzer, J. Fragemann, F. Jonske, M. Remppe, A. Abourayya, S. Malorodov, F. H. Bahnsen, C. Seibold, A. S. Santos, M. Lindo, A. Ferreira, F. Nensa, F. Hörst, A. Brehmer, L. Heine, J. Keyl, M.-S. Kim, M. Kamp, J. Kleesiek and J. Egger are with the Institute for Artificial Intelligence in Medicine (IKIM), University Hospital Essen (AöR), Girardetstraße 2, 45131 Essen, Germany. E-mails: Jianning.Li@uk-essen.de; Jan.Egger@uk-essen.de
- J. Li, A. Pepe, C. Gsaxner, Y. Jin, G. Luijten, N. Solak and J. Egger are with the Institute of Computer Graphics and Vision (ICG), Graz University of Technology, Inffeldgasse 16c, 8010 Graz, Austria.
- J. Li, A. Pepe, C. Gsaxner, Y. Jin, G. Luijten, N. Solak and J. Egger are with Computer Algorithms for Medicine Laboratory (Cafe), Graz, Austria.
- Y. Jin is with the Research Center for Connected Healthcare Big Data, ZhejiangLab, Hangzhou, Zhejiang, 311121 China.
- G. M. Melito is with the Institute of Mechanics, Graz University of Technology, Kopernikusgasse 24/IV, 8010 Graz, Austria.

## 1 INTRODUCTION

The success of deep learning in so many fields of applications [1], [2], [3] is in not small part due to the availability of large, high-quality datasets [4], such as *ImageNet* [5], *CIFAR* [6], and *a2d2* [7]. In computer vision, *Princeton ModelNet* [8], *ShapeNet* [9], etc., are the de facto benchmarks for numerous fundamental vision problems, such as 3D shape classification/retrieval, completion, reconstruction and segmentation [10], [11], [12], [13], [14], [15], [16]. Shape describes the geometries of 3D objects

and is one of the most basic concepts in computer vision. Common 3D shape representations include point clouds, voxel grids, meshes and implicit surface models (signed distance functions), which follow different data structures, cater for different algorithms but are convertible to each other [17].

These shape representations differ substantially from the medical imaging data (computed tomography, magnetic resonance imaging, positron emission tomography, ultrasound, X-ray) commonly used in clinical research. As

- X. Chen is with the Institute of Biomedical Manufacturing and Life Quality Engineering, State Key Laboratory of Mechanical System and Vibration, School of Mechanical Engineering, Shanghai Jiao Tong University, 800 Dongchuan Road, Shanghai, 200240, People's Republic of China.
- A. R. Memon is with the Department of Mechanical Engineering, Mehran University of Engineering and Technology, Jamshoro 76062, Sindh, Pakistan.
- A. R. Memon and X. Chen are with the Institute of Medical Robotics, Shanghai Jiao Tong University, Shanghai, People's Republic of China.
- J. S. Kirschke is with the Geschäftsführender Oberarzt Abteilung für Interventionelle und Diagnostische Neuroradiologie, Universitätsklinikum der Technischen Universität München, Ismaningerstr. 22, 81675 München, Germany.
- Ezequiel de la Rosa is with icometrix, Kolonel Begaultlaan 1b, 3012 Leuven, Belgium, and the Department of Informatics, Technical University of Munich, Boltzmannstraße 3, 85748 Garching bei München, Germany.
- S. Gatidis and T. Küstner are with the University Hospital of Tuebingen Diagnostic and Interventional Radiology Medical Image and Data Analysis (MIDAS.lab), Otfried-Müller-Str. 3, 72016 Tuebingen, Germany.
- D. G. Ellis and M. R. Aizenberg are with the Department of Neurosurgery, University of Nebraska Medical Center, Omaha, NE, 68198 USA.
- N. Shusharina is with the Division of Radiation Biophysics, Department of Radiation Oncology, Massachusetts General Hospital and Harvard Medical School, 55 Fruit St, Boston, Massachusetts 02114 USA.
- N. Heller is with the University of Minnesota, Minneapolis, MN 55455 USA.
- V. Andrearczyk and A. Depeursinge are with the Institute of Informatics, HES-SO Valais-Wallis University of Applied Sciences and Arts Western Switzerland, rue du Technopole 3, 3960 Sierre, Switzerland; A. Depeursinge is also with the Department of Nuclear Medicine and Molecular Imaging, Lausanne University Hospital (CHUV), Rue du Bugnon 46, 1005 Lausanne, Switzerland.
- M. Hatt is with LaTIM, INSERM, UMR 1101, Univ Brest, Brest, France.
- R. Dorent, T. Vercauteren, J. Shapey and A. Kujawa are with the King's College London, Strand, London WC2R 2LS, UK; R. Dorent is also with the Department of Neurosurgery, Brigham and Women's Hospital, Harvard Medical School, 75 Francis St, Boston, MA 02115 USA.
- S. Cornelissen and P. Langenhuizen are with Elisabeth-TweeSteden Hospital, Hilvarenbeekse Weg 60, 5022 GC Tilburg, Netherlands and the Video Coding & Architectures Research Group, Department of Electrical Engineering, Eindhoven University of Technology, Groene Loper 3, 5612 AE, Eindhoven, Netherlands.
- A. B. Hamadou and A. Rekik are with the Centre de Recherche en Numérique de Sfax, Laboratory of Signals, Systems, Artificial Intelligence and Networks, Technopôle de Sfax, 3021 Sfax, Tunisia, and Udini, 37 BD Aristide Briand, 13100 Aix-En-Provence, France.
- S. Pujades and E. Boyer are with Inria, Université Grenoble Alpes, CNRS, Grenoble INP, LJK, 38000 Grenoble, France.
- A. Sekuboyina is with the Department of Informatics, Technical University of Munich, Germany, Boltzmannstraße 3, 85748 Garching bei München, Germany.
- Maximilian Löffler is with the Universitätsklinikum Freiburg, Hugstetter Strasse 55, 79106 Freiburg, Germany.
- Hans Liebl is with the Department of Neuroradiology, Klinikum Rechts der Isar, Ismaninger Str. 22, 81675 Munich, Germany.
- P. F. Christ, H. B. Li and B. Menze are with the Department of Quantitative Biomedicine, University of Zurich, Winterthurerstrasse 190, 8057 Zurich, Switzerland.
- F. Bolelli, C. Grana and L. Lumetti are with the University of Modena and Reggio Emilia, Department of Engineering "Enzo Ferrari", Via Vivarelli 10, 41125, Modena, Italy.
- M. Kamp and A. Abourayya are with the Institute for Neuroinformatics, Ruhr University Bochum, Germany. M. Kamp is also with the Department of Data Science & AI, Monash University, Australia.
- C. Gsaxner, F. Hölzle and B. Puladi are with the Department of Oral and Maxillofacial Surgery, University Hospital RWTH Aachen, Pauwelsstraße 30, 52074 Aachen, Germany.
- V. Badeli is with the Institute of Fundamentals and Theory in Electrical Engineering, Graz University of Technology, 8010 Graz, Austria.
- K. Krieger, M. Gunzer and J. Chen are with the Leibniz-Institut für Analytische Wissenschaften-ISAS-e.V., 44139 Dortmund, Germany.
- M. Gunzer is with the Institute for Experimental Immunology and Imaging, University Hospital, University Duisburg-Essen, Hufelandstrasse 55, 45147 Essen, Germany.
- R. Röhrig and B. Puladi are with the Institute of Medical Informatics, University Hospital RWTH Aachen, Pauwelsstraße 30, 52074 Aachen, Germany.
- A. Jaus is with the Computer Vision for Human-Computer Interaction Lab, Department of Informatics, Karlsruhe Institute of Technology, Am Fasanengarten 5, 76131 Karlsruhe, Germany.
- A. S. Santos, M. Lindo, A. Ferreira and V. Alves are with the Center Algoritmi / LASI, University of Minho, Braga, 4710-057, Portugal.
- L. E. Podleska is with the Department of Tumor Orthopedics and Sarcoma Surgery, University Hospital Essen (AöR), Hufelandstraße 55, 45147 Essen, Germany.
- M. A. Fink is with the Clinic for Diagnostic and Interventional Radiology, University Hospital Heidelberg, Im Neuenheimer Feld 420, 69120 Heidelberg, Germany.
- K. Tserpes is with the Department of Informatics and Telematics, Harokopio University of Athens, 9 Omirou, 177 78, Tavros, Greece.
- E. A. Garza-Villarreal, T. Balducci and D. Angeles-Valdez are with the Institute of Neurobiology, Universidad Nacional Autónoma de México campus Juriquilla, Boulevard Juriquilla 3001, Juriquilla, Querétaro, 76230, México. D. Angeles-Valdez is also with the Department of Biomedical Sciences of Cells and Systems, Cognitive Neuroscience Center, University Medical Center Groningen, University of Groningen, Hanzeplein 1, 9713 GZ Groningen, Netherlands.
- S. Chatterjee and A. Nürnberger are with Data and Knowledge Engineering Group, Faculty of Computer Science, Otto von Guericke University Magdeburg, Universitätspl. 2, 39106 Magdeburg, Germany. S. Chatterjee is also with Genomics Research Centre, Human Technopole, Milan, Italy. A. Nürnberger is also with Centre for Behavioural Brain Sciences, Magdeburg, Universitätspl 2, 39106 Magdeburg, Germany.
- S. Elhabian is with the Scientific Computing and Imaging Institute, University of Utah, Utah, 72 South Central Campus Drive, Salt Lake City, 84112 USA.
- H. Lamecker is with 1000shapes GmbH, Hamerlingweg 5, 14167 Berlin, Germany.
- B. Paniagua and Dž. Zukić are with Medical Computing, Kitware Inc., Carrboro, North Carolina, 101 East Weaver St, Suite G4, 27510 USA.
- C. Wachinger is with the Lab for Artificial Intelligence in Medical Imaging, Department of Radiology, Technical University Munich, Ismaningerstr. 22, 81675 Munich, Germany.
- M. Urschler is with the Institute for Medical Informatics, Statistics and Documentation, Medical University Graz, Auenbruggerplatz 2, 8036 Graz, Austria.
- J. Wasserthal is with the Clinic of Radiology & Nuclear Medicine, University Hospital Basel, Petersgraben 4, 4031 Basel, Switzerland.
- L. Duong is with the Département de génie logiciel et des TI, École de technologie supérieure, 1100 Notre-Dame Ouest, Montréal (Québec) H3C 1K3, Canada.
- C. Davatzikos is with the Center for Biomedical Image Computing and Analytics, Penn Neurodegeneration Genomics Center, and Center for AI And Data Science For Integrated Diagnostics, University of Pennsylvania, Philadelphia, PA 19104 USA.

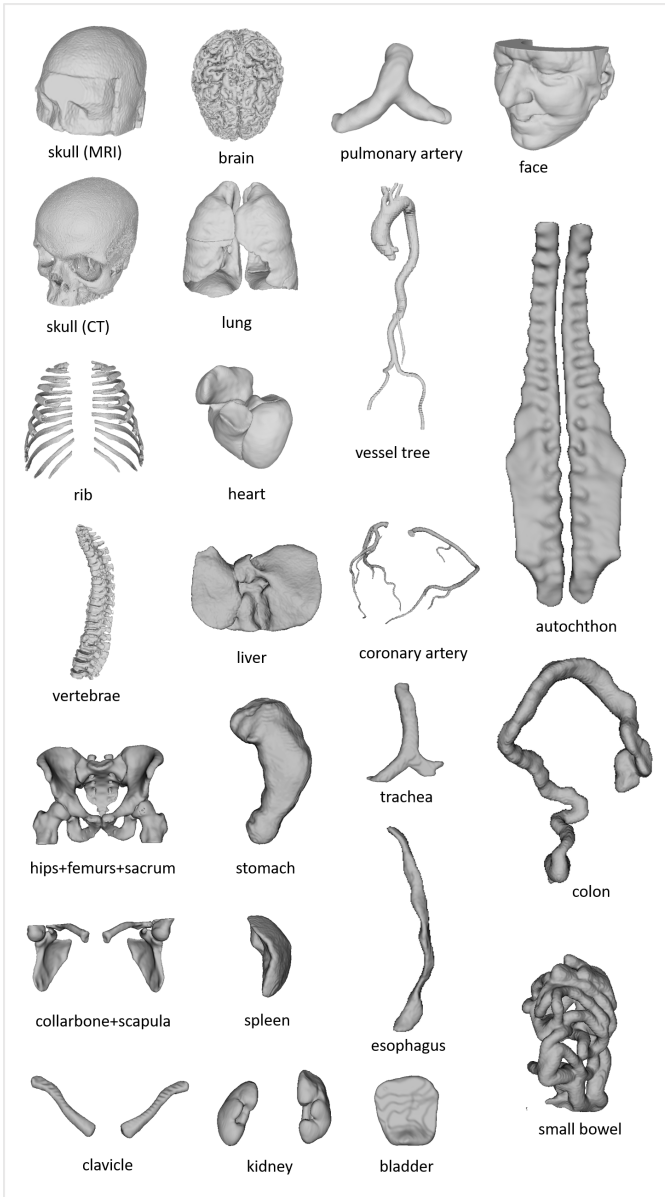


Fig. 1. Example shapes in *MedShapeNet*, including various bones (e.g., skulls, ribs and vertebrae), organs (e.g., brain, lung, heart, liver), vessels (e.g., aortic vessel tree and pulmonary artery) and muscles.

a result, the transferability of state-of-the-art (SOTA) vision algorithms to medical/clinical problems is limited, since vision methods developed on general 3D shapes are not directly transferable to volumetric, gray-scale medical data. Therefore, the community needs a large, high-quality shape database for medical imaging. With *MedShapeNet*, we provide a large-scale dataset of 3D medical shapes, i.e., voxel occupancy grid (VOR), mesh and point representations of human anatomies (e.g., liver, heart, lung, kidney, vertebrae, rib) - formats that advanced vision algorithms are compatible with [18] but are under-represented in current medical imaging research. While *ShapeNet* is comprised of 3D computer-aided design (CAD)

- Y. Zhang is with the Shanghai AI Laboratory, Yunjin Road, Shanghai, 200032, People's Republic of China.
- R. Gharlegghi and S. Beier are with the School of Mechanical and Manufacturing Engineering, UNSW, Sydney, 2052, NSW, Australia.
- A. Sowmya is with the School of Computer Science and Engineering, UNSW, Sydney, 2052, NSW, Australia.
- R. Souza is with the Advanced Imaging and Artificial Intelligence Lab, Electrical and Software Engineering Department, and the Hotchkiss Brain Institute, University of Calgary, Calgary, Canada.
- L. Rittner is with the Medical Image Computing Lab, School of Electrical and Computer Engineering (FEEC), University of Campinas, Campinas, Brazil.
- R. Frayne is with the Radiology and Clinical Neurosciences Departments, the Hotchkiss Brain Institute, University of Calgary, Calgary, Canada, and the Seaman Family MR Research Centre, Foothills Medical Center, Calgary, Canada.
- Y. Ji and P. Luo are with the University of Hongkong, Pok Fu Lam, Hong Kong, People's Republic of China.
- H. Salehi is with the Department of Artificial Intelligence in Medical Sciences, Faculty of Advanced Technologies in Medicine, Iran University Of Medical Sciences, Tehran, Iran.
- J. Pedrosa, C. Ferreira, A. Cunha and A. Campilho are with the Institute for Systems and Computer Engineering, Technology and Science (INESC TEC), Porto, Portugal; J. Pedrosa, C. Ferreira and A. Campilho are also with Faculty of Engineering of the University of Porto (FEUP), Porto, Portugal. A. Cunha is also with Universidade of Trás os Montes and Alto Douro (UTAD), Vila Real, Portugal.
- G. Aresta is with the Christian Doppler Lab for Artificial Intelligence in Retina, Department of Ophthalmology and Optometry, Medical University of Vienna, Austria.
- Y. Suter and M. Reyes are with ARTORG Center for Biomedical Engineering Research, University of Bern, Bern, Switzerland. M. Reyes is also with the Department of Radiation Oncology, University Hospital Bern, University of Bern, Switzerland.
- J. Garcia is with the Center for Biomedical Image Computing and Analytics (CBICA), Perelman School of Medicine, University of Pennsylvania.
- A. Lalonde is with ICMUB laboratory, CNRS UMR 6302 Faculty of Medicine, University of Burgundy, 7 Bld Jeanne d'Arc, BP 87900, 21079 Dijon, cedex, France and Medical Imaging Department - University Hospital of Dijon, 1 Bld Jeanne d'Arc, BP 77908, 21079 Dijon Cedex, France.
- E. Audenaert is with the Department of Human Structure and Repair, Ghent University, Corneel Heymanslaan 10, 9000 Ghent, Belgium.
- C. Krebs is with the Department of Cellular and Physiological Sciences, Life Sciences Centre, 1544 - 2350 Health Sciences Mall, University of British Columbia, Vancouver, British Columbia, V6T 1Z3 Canada.
- E. Vereecke and T. V. Leeuwen are with the Department of Development & Regeneration, KU Leuven Campus Kulak, Etienne Sabbelaan 53, 8500 Kortrijk, Belgium.
- M.-S. Kim and F. Nensa are with the Institute of Diagnostic and Interventional Radiology and Neuroradiology, University Hospital Essen (AöR), Hufelandstraße 55, 45147 Essen, Germany.
- J. Kleesiek is with German Cancer Consortium (DKTK), Partner Site Essen, Hufelandstraße 55, 45147 Essen, Germany, and the Department of Physics, TU Dortmund University, August-Schmidt-Str. 4, 44227 Dortmund, Germany.
- M. Kamp, F. Hörst, M.-S. Kim, J. Kleesiek and J. Egger are with the Cancer Research Center Cologne Essen (CCCE), University Medicine Essen (AöR), Hufelandstraße 55, 45147 Essen, Germany.
- P. F. Hoyer is with the Department of Pediatrics II, University Hospital Essen, Hufelandstraße 55, 45147 Essen, Germany.
- O. Basu is with the Department of Pediatrics III, University Hospital Essen, University Medicine Essen, Hufelandstraße 55, 45147 Essen, Germany.
- T. Maal is with the 3D Imaging Lab, Radboud University Nijmegen Medical Centre, Geert Grooteplein 10, 6525 GA, Nijmegen, The Netherlands.
- M. J. H. Witjes is with the Department of Oral and Maxillofacial Surgery, University of Groningen, University Medical Center Groningen, Hanzplein 1 BB70, 9713 GX Groningen, The Netherlands.
- O. Basu and J. Egger are with the Center for Virtual and Extended Reality in Medicine (ZöRM), University Hospital Essen, University Medicine Essen, Hufelandstraße 55, 45147 Essen, Germany.
- J. Ma is with the Department of Laboratory Medicine and Pathobiology, University of Toronto, Toronto, ON M5S 1A8 Canada; Peter Munk Cardiac Centre, University Health Network, 585 University Ave, Toronto, ON M5G 2N2, Canada; Vector Institute, 661 University Ave Suite 710, Toronto, ON M5G 1M1, Canada.

models of real-world objects (e.g., *plane, car, chair, desk*), the medical shapes from *MedShapeNet* are directly extracted from the imaging data of real patients (e.g., Figure 1). *MedShapeNet* by itself is therefore not only a unique dataset for medical imaging but also an ideal alternative and complement to the common shape benchmarks, like *ShapeNet* [9], for computer vision research, such as domain adaptation (CAD → real-world) [19].

*MedShapeNet* makes an effort to bridge the gap between the medical imaging and computer vision community, and to promote the translation of vision algorithms to medical applications. The benefits are reciprocal: it makes it easier for vision researchers to work on medical applications and encourages medical researchers to revisit and adopt shape-based methods from computer vision for medical problems. The MICCAI society, a leading professional organization in medical image computing and computer assisted intervention, has initiated a special interest group in *Shape in Medical Imaging (ShapeMI*<sup>1</sup>), suggesting the significance of the role shape-based methods play in this field. Table 1 provides a non-inclusive list of organizations/events that focus on promoting shape methods for medical applications.

*MedShapeNet* includes diverse anatomical shapes and can facilitate the development and evaluation of data-driven, shape-based methods for a variety of medical as well as vision problems. On the one hand, numerous existing medical problems can be solved using shape-based methods. A typical example is cranial implant design [20], [21], [22], [23], [24], [25], [26], which is commonly formulated as a shape completion problem and solved using well established completion methods from computer vision [27], [28], [29], [30], [31]. The same concept can be conveniently extended to the design of other bone grafts (e.g., ribs, spine) and even artificial organs (e.g., liver, heart, kidney) for 3D bio-printing. Another representative example is statistical shape modeling (SSM), which has long been employed for medical image segmentation [32], [33] and anatomy modeling [34], [35], [36], [37], [38], [39], [40], [41] by the community. Shape priors and/or geometric constraints of various anatomies (e.g., aorta, skull) can also be derived from *MedShapeNet* for downstream segmentation and reconstructive tasks [42], [43], [44], [45], [46], [47]. Last but not least, *MedShapeNet* offers opportunities to explore shape-based methods for problems that are traditionally solved based on gray-scale medical images, such as disease diagnosis. Switching to medical shapes allows one to exploit more computationally efficient and geometry-oriented methods, such as sparse convolutional neural networks [48], for the medical diagnostic problems. On the other hand, anatomical shapes are also commonly used for general computer vision research aimed at (primarily) non-medical applications, such as facial modeling [49], [50] and internal anatomy (e.g., skeleton, organs) inference [51], [52]. *MedShapeNet* also contains pathological anatomies, such as tumorous brains, kidneys and livers (Figure 3), as well as brains from patients with cognitive impairment (e.g., Alzheimer’s disease) or substance use disorder (e.g., alcohol use disorder - AUD, cocaine use disorder - CUD). Machine learning models can be trained for automatic abnormality

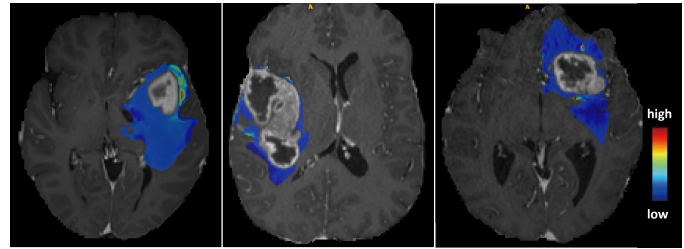


Fig. 2. The *predictive maps* overlaid onto patients’ MRI scans. The *predictive maps* are color-coded to indicate high or low probability of tumor infiltration.

detection using such shape data. Through statistical analysis and comparison, geometric differences between normal and pathological anatomies can be quantified, which facilitates automatic diagnostics and the discovery of geometric biomarkers [53], [54]. *MedShapeNet* can also be used for anatomy education, as it provides the 3D models of a variety of human anatomies, both normal and pathological, that can be 3D printed or used digitally in an extend reality, such as augmented reality (AR), environment [55], [56]. *MedShapeNet* also benefits researchers who want to study the shape variations of a certain anatomy, but do not have access to the 3D scans and lack the resources to create the segmentations manually.

The manuscript is organized as follows. Section 2 discusses the shape and voxel features in medical imaging, and the motivation of this project. Section 3 introduces the different sources from which the shape data in *MedShapeNet* are derived. Section 4 presents several interesting use cases of *MedShapeNet*, and demonstrates how *MedShapeNet* can be used in real-world applications in computer vision, medical imaging and augmented-reality. Section 5 introduces the online interface of *MedShapeNet* and how to use it. Section 6 concludes the manuscript and discusses the future work.

## 2 SHAPE AND VOXEL FEATURES

Shapes describe objects’ geometries, provide a foundation for computer vision, and serve as a computationally efficient way to represent images despite not capturing voxel features like gray-scale medical images.

Even though the main motivation behind *MedShapeNet* is to emphasize the importance of shape characteristics, such as jaggedness, volume, elongation, etc., over voxel features, and to show that voxel features are redundant for certain tasks, learning algorithms might require additional (voxel) information to construct a decision boundary in some situations. For example, liver and brain tumors can have a noticeable impact on the morphology and/or volume of the corresponding organ (Figure 3), so that learning algorithms can easily distinguish between healthy and tumorous organs based on these shape features alone. However, for pathologies that do not induce (obvious) morphological changes, such as neurodegenerative diseases (e.g., mild cognitive impairment or Alzheimer’s disease), shape-related features might not be discriminative enough for learning algorithms to converge during training. In the latter case, adding additional voxel features is beneficial.

1. <https://shapemi.github.io/>

TABLE 1  
A Non-inclusive List of Organizations/Events Featuring Shape Methods for Medical Applications

Sources (link)	Description	Category
Zuse Institute Berlin (ZIB) <a href="#">↗</a> , <a href="#">↗</a>	shape-informed medical image segmentation and shape priors in medical imaging	research group
ShapeMI <a href="#">↗</a>	shape processing/analysis/learning in medical imaging	MICCAI workshop
SIG <a href="#">↗</a>	shape modeling and analysis in medical imaging	MICCAI special interest group (SIG)
Autolmplant I, II <a href="#">↗</a> , <a href="#">↗</a>	skull shape reconstruction and completion	MICCAI challenge
WiSh <a href="#">↗</a>	women in Shape Analysis, shape modeling	professional organization
STACOM <a href="#">↗</a>	statistical atlases and computational models of the heart	MICCAI workshop
SAMIA <a href="#">↗</a>	shape analysis in medical image analysis	book
CIBC <a href="#">↗</a>	image and geometric analysis	research group
GeoMedIA <a href="#">↗</a>	geometric deep learning in medical image analysis	MICCAI-endorsed workshop
IEEE TMI <a href="#">↗</a>	geometric deep learning in medical imaging	journal special issue
PMLR <a href="#">↗</a>	geometric deep learning in medical image analysis	proceedings
Elsevier <a href="#">↗</a>	Riemannian geometric statistics in medical image analysis	book
Springer <a href="#">↗</a>	geometric methods in bio-medical image processing	proceedings

Refer to Section 4.2.4 for preliminary experimental evidence of these assumptions.

Another example where voxel features are essential is when accurate spatial location is necessary, such as during precision tumor therapy. In [57], the authors show that spatial *predictive maps* that indicate areas of early tumor (glioblastoma) recurrence and infiltration can be derived from preoperative MRIs, and used for targeted radiotherapy [58]. The *predictive maps* are generated via a voxel-wise classification of the gray-scale tumor voxels. As shown in Figure 2, the *predictive map* shows the spatial pseudo-probability of tumor infiltration. Areas with high probability have higher risks of tumor recurrence after resection.

How to optimally combine voxel features with shapes is an interesting topic requiring further investigation. With *MedShapeNet*, one can investigate (1) to what degree a pathological condition, such as tumor, Alzheimer’s disease (AD) and substance use disorder (SUD) can be captured by the shape features of the organs affected (e.g., the brain), determined by the convergence of a classifier when trained on shape features alone; (2) what shape features are the most discriminative of a pathology and how to calculate them [59]; (3) how to effectively integrate voxel features into shapes when shape features alone are not sufficient; and (4) if there are associations between voxel and shape features? In the example of [57], one can ask whether the high infiltration voxels induce morphological changes to the tumor (boundaries) correspondingly.

To answer these questions and support future research on this endeavor, *MedShapeNet* links the ‘source of shapes’ i.e., the original medical images with its shape collections, so that the voxel information of a specific shape can be retrieved whenever needed. The following section describes the ‘source of shapes’ in detail.

### 3 SOURCES OF SHAPES

The anatomical shapes in *MedShapeNet* are converted from binary segmentation masks (voxel occupancy grids) of organs, bones, vessels, muscles, etc., using *Marching Cubes* [105]. We collect the segmentation masks from different sources, where the segmentation masks are either generated automatically by a segmentation network (e.g., in the case of *TotalSegmentator*) or manually, as those of the ground truth in the training set of a public medical image segmentation



challenge [106], [107], [108]. Some of the masks are from our own datasets. Table 2 summarizes the data sources, such as *TotalSegmentator* [60], *MUG500+* [61], the *Human Connectome Projects* (HCP) [62] and the aortic vessel tree (AVT) dataset [64]. Miscellaneous sources include the *Skull-stripped MRI Glioblastoma Multiforme (GBM) Dataset* [65] and the *Medical Augmented Reality Facial Data Collection* [63], as shown in Figure 1. Note that different sources could contain the same anatomy. For example, both the *TotalSegmentator* and VerSe [67] datasets include vertebrae. The anatomical shapes in *MedShapeNet* are provided as meshes (.stl), points and voxel occupancy grids to cater for different vision algorithms.

**Privacy and ethics considerations:** The *MedShapeNet* database is created exclusively for research and educational purposes. The majority of the source datasets are Creative Commons (CC)- or CC BY 4.0-licensed (Refer to Table 2 for data licenses). Publicly sharing medical data is encouraged but regulated at the same time due to potential privacy concerns [109], [110]. *MedShapeNet* does not include gray-scale medical images, which contain patient-specific information, such as racial identity, that can be inferred using an identity recognition network [111], [112]. Training on shape data encourages a machine learning model to focus on learning discriminative geometric features rather than learning irrelevant patients’ identities, which may undermine the robustness and trustworthiness of the machine learning model and lead to identity-driven bias. Publicly sharing gray-scale head CT and MRI scans bears the risk of exposing the facial profiles of the patients [113]. *MedShapeNet* removes the gray values in head CTs and MRIs and shares only the skulls, making the reidentification of the patients more difficult. Existing facial models (Figure 1) are CC BY 4.0-licensed [63]. The original study was approved by the ethics committee, and participants also provided their informed consent. The HCP database is not CC-licensed but its use terms permit the redistribution of the original and derived data. *MedShapeNet* only shares the binarized version of the brains extracted from the original HCP MRIs, as seen in Figure 1.

#### 3.1 TotalSegmentator

The *TotalSegmentator* dataset from Wasserthal et al. [60] includes over 1000 CT scans and the corresponding segmentations of 104 anatomical structures covering the

TABLE 2  
Summary of the Sources of the Anatomical Shapes in *MedShapeNet*

Sources	Description	URLs	Dataset License
<i>TotalSegmentator</i> [60]	various anatomical structures	<a href="https://doi.org/10.5281/zenodo.6802613">https://doi.org/10.5281/zenodo.6802613</a>	CC BY 4.0
<i>MUG500+</i> [61]	healthy and craniotomy CT skulls	<a href="https://doi.org/10.6084/m9.figshare.9616319">https://doi.org/10.6084/m9.figshare.9616319</a>	CC BY 4.0
<i>HCP</i> [62]	paired brain-skull extracted from MRIs	<a href="https://humanconnectome.org/">https://humanconnectome.org/</a>	Data Use Terms 
Facial Models [63]	facial models for augmented reality	<a href="https://doi.org/10.6084/m9.figshare.8857007.v2">https://doi.org/10.6084/m9.figshare.8857007.v2</a>	CC BY 4.0
AVT [64]	aortic vessel trees	<a href="https://doi.org/10.6084/m9.figshare.14806362">https://doi.org/10.6084/m9.figshare.14806362</a>	CC BY 4.0
MRI GBM [65]	brain and GBM extracted from MRIs	<a href="https://doi.org/10.6084/m9.figshare.7435385.v2">https://doi.org/10.6084/m9.figshare.7435385.v2</a>	CC BY 4.0
SkullFix [66]	complete and artificially defected skulls	<a href="https://autoimplant2021.grand-challenge.org/Dataset/">https://autoimplant2021.grand-challenge.org/Dataset/</a>	CC BY 4.0
SkullBreak [66]	complete and artificially defected skulls	<a href="https://doi.org/10.6084/m9.figshare.14161307.v1">https://doi.org/10.6084/m9.figshare.14161307.v1</a>	CC BY 4.0
VerSe [67]	large scale vertebrae segmentation	<a href="https://github.com/anjany/verse">https://github.com/anjany/verse</a>	CC BY 4.0
KiTS21 [68]	kidney and kidney tumor segmentation	<a href="https://github.com/neheller/kits21">https://github.com/neheller/kits21</a>	MIT
BraTS [69], [70], [71]	brain tumor segmentation	<a href="https://www.synapse.org/#!Synapse:syn27046444/wiki/">https://www.synapse.org/#!Synapse:syn27046444/wiki/</a>	-
3DTeethSeg [72], [73]	3D Teeth Scan Segmentation	<a href="https://github.com/abenhamadou/3DTeethSeg22_challenge">https://github.com/abenhamadou/3DTeethSeg22_challenge</a>	CC BY NC ND 4.0
HECKTOR [74], [75]	head and neck tumor segmentation	<a href="https://hecktor.grand-challenge.org/">https://hecktor.grand-challenge.org/</a>	-
KiTS [68]	kidney and kidney tumor segmentation	<a href="https://kits21.kits-challenge.org/">https://kits21.kits-challenge.org/</a>	-
Crossmoda [76], [77]	brain tumor and Cochlea segmentation	<a href="https://zenodo.org/record/6504722">https://zenodo.org/record/6504722</a>	CC BY 4.0
LITS [78]	liver tumor segmentation	<a href="https://competitions.codalab.org/competitions/17094">https://competitions.codalab.org/competitions/17094</a>	-
ISLES22 [79]	ischemic stroke lesion segmentation	<a href="https://isles22.grand-challenge.org/">https://isles22.grand-challenge.org/</a>	CC-BY-4.0
GLISRT [80], [81], [82]	brain structures	<a href="https://doi.org/10.7937/TCIA.T905-ZQ20">https://doi.org/10.7937/TCIA.T905-ZQ20</a>	TCIA Restricted 
autoPET [83], [84], [85], [86]	whole-body segmentations	<a href="https://autopet.grand-challenge.org/">https://autopet.grand-challenge.org/</a>	CC BY 4.0
AbdomenCT-1K [87]	abdomen organs	<a href="https://github.com/JunMa11/AbdomenCT-1K">https://github.com/JunMa11/AbdomenCT-1K</a>	-
FLARE [87], [88], [89], [90]	13 Abdomen organs	<a href="https://flare22.grand-challenge.org/">https://flare22.grand-challenge.org/</a>	-
ToothFairy [91], [92]	inferior alveolar canal	<a href="https://toothfairychallenges.github.io/">https://toothfairychallenges.github.io/</a>	CC BY SA
ASOCA [93], [94]	normal and diseased coronary arteries	<a href="https://asoca.grand-challenge.org/">https://asoca.grand-challenge.org/</a>	-
Calgary-campinas [95]	brain structure segmentations	<a href="https://portal.conp.ca/dataset?id=projects/calgary-campinas">https://portal.conp.ca/dataset?id=projects/calgary-campinas</a>	-
SUDMEX CONN [96]	healthy and (cocaine use disorder) CUD brains	<a href="https://openneuro.org/datasets/ds003346/versions/1.1.2">https://openneuro.org/datasets/ds003346/versions/1.1.2</a>	-
AMOS [97]	abdominal multi organs in CT and MRI	<a href="https://zenodo.org/record/7155725#.YOOCOxBztM">https://zenodo.org/record/7155725#.YOOCOxBztM</a>	-
LNDb [98], [99]	lung nodules	<a href="https://lndb.grand-challenge.org/">https://lndb.grand-challenge.org/</a>	CC BY NC ND 4.0
PROMISE [100]	prostate MRI segmentation	<a href="https://zenodo.org/record/8014041">https://zenodo.org/record/8014041</a>	-
TCGA-GBM [71]	glioblastoma	<a href="https://www.nature.com/articles/sdata2017117">https://www.nature.com/articles/sdata2017117</a>	-
EMIDEC [101], [102]	normal and pathological (infarction) myocardium	<a href="https://emidec.com/segmentation-contest">https://emidec.com/segmentation-contest</a>	CC BY NC SA 4.0
CT-ORG [103]	multiple organ segmentation	<a href="https://doi.org/10.6084/m9.figshare.13055663">https://doi.org/10.6084/m9.figshare.13055663</a>	CC0 1.0
LUMIERE [104]	longitudinal glioblastoma	<a href="https://doi.org/10.6084/m9.figshare.c.5904905.v1">https://doi.org/10.6084/m9.figshare.c.5904905.v1</a>	CC BY NC

whole body, which are generated automatically by a nnUNet-based segmentation network [114].

### 3.2 Human Connectome Projects (HCP)

The *1200 Subjects Data Release* from the *Human Connectome Projects* (HCP) includes 1113 structural 3T head MRI scans of healthy young adults. From each MRI scan, the segmentation masks of the skull and the brain are extracted using the *Cortical Surface Extraction* script provided by *BrainSuite* (<http://brainsuite.org/>). Due to the highly complex brain geometries, the size of a brain mesh converted from a segmentation mask exceeds one Gigabyte. Considering the limited space for storing the shape data, we downsized the brain masks by a factor of 1.6 before converting them to meshes. This course of action reduces the size of each brain shape to 200 MB - 500 MB at the cost of reduced shape quality. A example of such brain shape is shown in Figure 1.

### 3.3 MUG500+

The *MUG500+* dataset contains the binary segmentation masks and meshes of 500 healthy human skulls and 29 craniectomy skulls with surgical defects [61]. The skull masks are segmented from head CT scans by thresholding.

### 3.4 SkullBreak/SkullFix

The *SkullBreak/SkullFix* dataset includes the binary segmentation masks of healthy human skulls and the corresponding skulls with artificial defects. The binary skull masks are segmented from head CT scans from the *CQ500* dataset (<http://headctstudy.que.ai/dataset>), using thresholding, similar to *MUG500+* [61].

### 3.5 AVT

The aortic vessel tree (AVT) dataset [64] contains 56 computed tomography angiography (CTA) scans of healthy aorta as well as the segmentation masks of the corresponding aortic vessel trees, including the aorta, aortic arch, branch and iliac arteries, as shown in Figure 1.

### 3.6 VerSe

The *large scale vertebrae segmentation (VerSe)* challenge [67], [115] provides the segmentation masks of vertebrae from around 210 subjects [116], [117]. 2745 vertebra shapes are generated from the challenge dataset.

### 3.7 ASOCA

The *automated segmentation of coronary arteries (ASOCA)* challenge provides the manual segmentations of 20 normal and 20 diseased coronary arteries [94].

### 3.8 3DTeethSeg

Automated teeth localization, segmentation, and labeling from intra-oral 3D scans are crucial tasks in modern dentistry, significantly improving dental diagnostics, treatment planning, and population-based studies on oral health. Before initiating any orthodontic or restorative treatment planning, it is essential for a CAD system to accurately segment and label each instance of teeth in the 3D dental scan. This eliminates the need of time-consuming manual adjustments by the dentist. To address this need, the *3D Teeth Scan Segmentation and Labeling Challenge (3DTeethSeg)* [72], [73] was organized in conjunction with

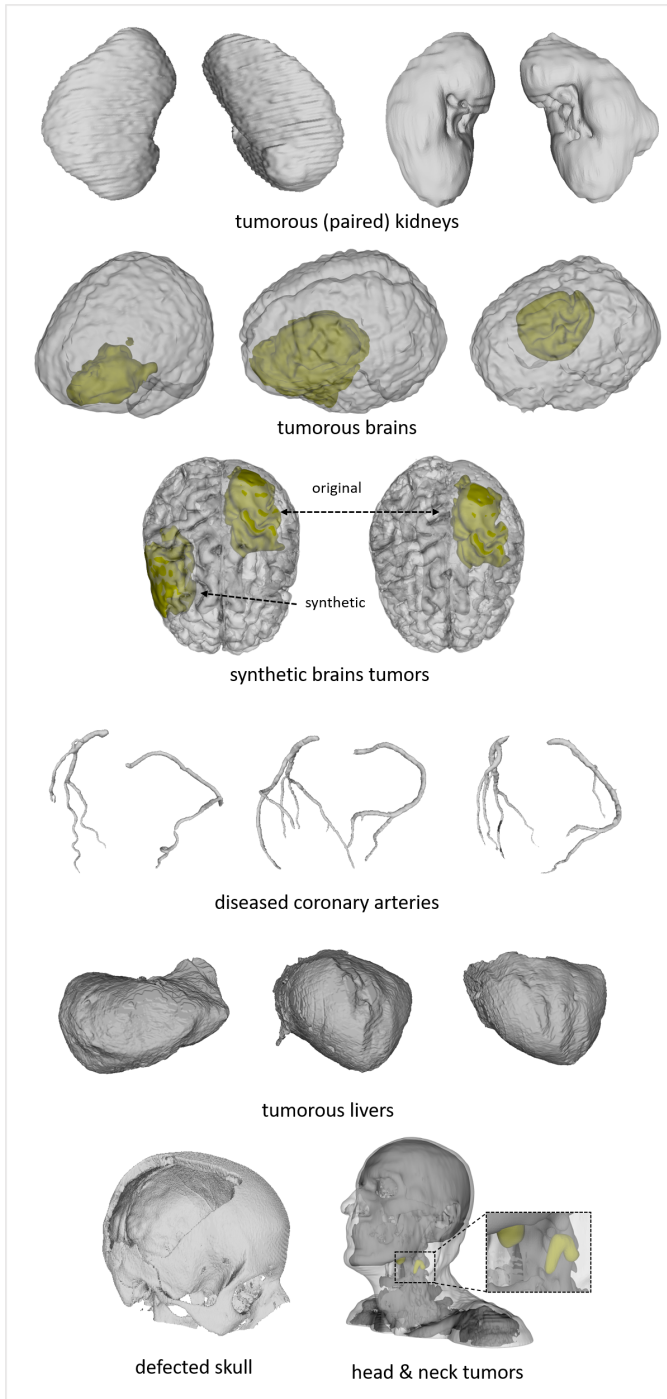


Fig. 3. Example pathological shapes in *MedShapeNet*, including tumorous kidney (paired), brain (with real and synthetic tumors), liver and head & neck, as well as diseased coronary arteries. For illustration purpose, the opacity of some shapes is reduced to reveal the underlying tumors. We can study the effects of tumors on the morphological changes of an anatomy (e.g., brain) using such pathological data.

the International Conference on Medical Image Computing and Computer Assisted Intervention (MICCAI) in 2022. This challenge provides the upper and lower intra-oral 3D scans of 900 subjects, along with the corresponding manual annotations for teeth segmentation and labeling tasks. The data annotation was performed in collaboration with clinical evaluators with more than 10 years of expertise in orthodontistry, dental surgery, and endodontics. A preliminary benchmark of state-of-the-art methods for the challenge can be found in [72].

### 3.9 LNDb

The data from the *automatic lung cancer patient management* (LNDb) challenge [98], [99] comprises lung nodule segmentations performed by five radiologists on low-dose computed tomography images within the scope of lung cancer screening. A total of 861 lung nodule segmentation masks are publicly available, corresponding to 625 individual nodules segmented on 204 CTs. Radiologists were asked to independently screen each CT and identify all pulmonary nodules and segment those with an in-plane dimension larger than or equal to 3mm. No consensus or review between radiologists was performed, meaning that there is a variable number of segmentations per nodule (between 1 and 3).

### 3.10 EMIDEC

The Emidec (automatic Evaluation of Myocardial Infarction from Delayed-Enhancement Cardiac MRI) dataset is composed of 150 exams with delayed enhancement-MRI (or DE-MRI) images in short axis orientation covering the left ventricle from normal cases or patients with myocardial infarction, with the contouring of the myocardium and diseased areas (if present) from experts in the domains [101], [102]. The database is composed of the imaging exam and the associated clinical information. The targeted cohort is any patient admitted in a cardiac emergency department with symptoms of a heart attack. Indeed, DE-MRI is a method of choice to evaluate the extent of myocardial infarction, and by extension, to assess viable tissues after an injury. The images are acquired roughly 10 minutes after the injection of a gadolinium-based contrast agent, and then the fibrotic area appears bright in T1-weighted DE-MRI whereas normal tissue appears dark. There is an unbalanced distribution between normal (1/3) and pathological (2/3) cases, corresponding roughly to real life in an MRI department. This dataset was available as part of the Emidec challenge organized in conjunction with the STACOM workshop during the MICCAI conference in 2020 [57]. Even if the data are freely available for research topic, the owner stays the University Hospital of Dijon (France)

### 3.11 ToothFairy

Dental implant placement within the jawbone is a routinely executed surgical procedure, which can become complex due to the local presence of the Inferior Alveolar Nerve (IAN) crossing the homonymous osseous structure (the Inferior Alveolar Canal, IAC in short). In particular, the nerve is in close relation to the roots of molars, and its



Fig. 4. Illustration of 3D models of medical instruments used in oral and cranio-maxillofacial surgeries. The 3D models are obtained using structured light 3D scanners (Artec Leo from Artec3D and AutoScan Inspec from Shining 3D). Instrument models can be retrieved by the search query *instrument* via the *MedShapeNet* web interface. Image taken from <https://xrlab.ikim.nrw/>.

position must thus be carefully detailed before the surgical removal. As avoiding contact with the IAN is a primary concern during these operations, segmentation plays a key role in surgical preparations. With the goal of pushing the development of deep learning frameworks to automatically segment the IAC, the *ToothFairy* dataset has been released by “ToothFairy: A Cone-beam Computed Tomography Segmentation Challenge” [92] organized within MICCAI 2023. *ToothFairy* extends the previously released Maxillo dataset [91], [118], [119], and it comprises 443 dental scans, captured using the NewTom/NTVGiMK4 CBCT scanner, operating at 3 mA and 110 kV, with a voxel size of  $0.3 \text{ mm}^3$ . The scans have been acquired with an intra-slice distance of 0.3 mm, yielding volumes with shapes ranging from (148, 265, 312) to (169, 342, 370) across the Z, Y, and X axes, respectively. The voxel values, represented in Hounsfield Units (HU), span from  $-1000$  to  $5264$ . The dataset includes 2D sparse annotations for all 443 volumes, while only a subset of 153 volumes features detailed 3D voxel-level annotations of the IAC. The ground-truth annotations of the IAC have been produced by a team of five experienced maxillofacial surgeons using an ad-hoc developed tool that leverages different computer vision techniques to assist the user during the annotation [120], [121]. An additional test-set of 50 CBCT volumes has been acquired using a standard CBCT scanning protocol (i-CAT, 3D Imaging System, Imaging Sciences International Inc, Hatfield, PA, USA) in “Extended Field” modus (FOV: 16cm diameter/22 cm height; scan time:  $2 \times 20s$ ; voxel size: 0.4 mm). These data represent the *ToothFairy* challenge evaluation dataset and, in this case, only the ground-truth annotations are made available.

### 3.12 HECKTOR

The training set of the *HEAd and neCK TumOR segmentation and outcome prediction* (HECKTOR) challenge [74], [75] comprises 524 3D FDG-PET/CT images from seven hospitals with manual primary tumor and metastatic lymph nodes contours. The data originates from FDG-PET and low-dose non-contrast-enhanced CT images (acquired with combined PET/CT scanners) of the H&N region of patients with oropharyngeal H&N cancer. The training set of the HECKTOR challenge is used for *MedShapeNet*.

### 3.13 autoPET

Similar to *TotalSegmentor*, whole-body segmentations are extracted from the PET/CT dataset provided by the AutoPet challenge [84], [86], using an semi-supervised segmentation network [83], [122], [123]. The autoPET dataset itself comes from cancer patients and also includes the manual segmentations of whole-body tumor lesions. It should be noted that the morphologies of some of the anatomies might be affected due to the existence of tumors.

### 3.14 Calgary-Campinas

The Calgary-Campinas (CC) dataset [95] consists of T1 magnetic resonance imaging (MRI) volumes acquired in 359 presumed healthy subjects on scanners from three different vendors (GE, Philips, and Siemens) and at two magnetic field strengths (1.5 T and 3 T). Data were obtained using T1-weighted 3D imaging sequences (3D MP-RAGE (Philips, Siemens), and a comparable T1-weighted spoiled gradient echo sequence (GE)) designed to produce high-quality anatomical data with  $1 \text{ mm}^3$  voxels. Age and gender for all subjects were known (176 M: 183 F,  $53.5 \pm 7.8$  years, min:18 years, max: 80 years), however information about



subject ethnicity was not available. Probabilistic brain masks were obtained by combining the output of eight automated brain segmentation algorithms [124], [125], [126], [127], [128], [129], [130], [131] using the Simultaneous Truth and Performance Level Estimation (STAPLE) algorithms [132]. The quality of the brain masks was validated against 12 manual brain segmentations obtained in a stratified manner across vendor, magnetic field, and subject sex combinations. The CC dataset has been used to investigate brain extraction models [133], [134], domain shift and adaptation in brain MRI [135], [136], as well as MRI reconstruction [137], [138].

### 3.15 AMOS

The AMOS dataset [97], both diverse and robust, includes 500 CT and 100 MRI images gathered from a variety of scanners and locations. It covers 15 distinct categories of abdominal organs: the spleen, right kidney, left kidney, gallbladder, esophagus, liver, stomach, aorta, inferior vena cava, pancreas, right adrenal gland, left adrenal gland, duodenum, bladder, and prostate/uterus. The images were predominantly collected from patient examinations involving abdominal tumors or other abnormalities.

### 3.16 AbdomenCT-1K and FLARE

The AbdomenCT-1K dataset includes the manual segmentations of the liver, kidney, spleen, and pancreas from over 1000 CT scans [87]. A subset of the dataset was used in the *fast and low-resource semi-supervised abdominal organ segmentation* (FLARE) challenge, which provides the manual segmentation of 13 abdomen organs, including the liver, spleen, pancreas, right kidney, left kidney, stomach, gallbladder, esophagus, aorta, inferior vena cava, right adrenal gland, left adrenal gland, and duodenum [88], [89]. Note that some of the CT scans are acquired from cancer patients. Tumors can affect the morphologies of these organs.

### 3.17 ISLES

The *ischemic stroke lesion segmentation* (ISLES) challenge [79] provides a dataset comprising of 250 brain MRIs along with binary masks depicting stroke infarctions. The dataset encompasses diverse brain lesions in terms of volume, location, and stroke pattern. The manually delineated segmentation masks are derived by refining pre-segmentations obtained using a 3D UNet [139].

### 3.18 Synthetic Anatomical Shapes

Generative adversarial networks (GANs) are capable of generating realistic 3D data [140]. Besides real anatomical shapes, *MedShapeNet* also includes synthetic shapes generated by GANs, which can be used for augmenting the dataset in deep learning-based tasks. In *MedShapeNet*, we use GANs to generate synthetic tumors for 27390 real brains, as shown in Figure 3. These synthetic brain masks can be used in combination with the original tumor labels to train a tumor segmentation network.

### 3.19 Medical Instrument

Besides anatomical shapes, *MedShapeNet* also contains the 3D models of medical instruments used primarily in oral and cranio-maxillofacial surgeries, such as the drill bits, scalpel and chisel, as shown in Figure 4. The 3D instrument models are obtained by scanning the corresponding instruments manually using two structured-light-based 3D scanners, namely, Autoscan Inspec (Shining 3D Corporation, Hangzhou, Zhejiang, China) and Artec Leo (Artec3D, Senningerberg, Canton Luxembourg, Luxembourg). The initial scans are post-processed (e.g., noise removal) using proprietary software, *Ultrascan version 2.0.0.7* and *Artec Studio 17 Professional*, before they are incorporated into the database. These instrument models can be used for surgical tool tracking (detection, classification) in augmented reality (AR) and mixed reality (MR) [55] for medical education and research.

### 3.20 Pathological Shapes

To increase the variability of the shape collections, *MedShapeNet* contains not only normal/healthy anatomical shapes, such as the kidneys from *TotalSegmentor* and the brains from *HCP*, but also pathological ones, which are derived from patients diagnosed with a specific pathological condition, such as tumor (liver, kidney, etc) and CUD (SUDMEX CONN, Table 2). Figure 3 shows the tumorous kidneys, brains, livers and head & neck, as well as diseased coronary arteries from different sources. We also use generative adversarial networks (GANs) to generate synthetic brain tumors, as shown in Figure 3.

## 4 ANNOTATION AND USE CASES

*MedShapeNet* provides annotations in the form of paired data. Large, high-quality, paired data are valuable assets in computer vision research [51], [141], as they facilitate supervised training of machine learning models and promise SOTA results. For example, Yu, J. et al. [141] curated a dataset, *CelebV-Text*, containing facial text-video pairs, which can be used for text-driven generation of face-centric videos. Similarly, Xing, J. et al. [142] used BIWI [143] and VOCASET [144], datasets containing paired audio (e.g., speech)-visual (e.g., facial expressions/motions) sequences, for speech-driven 3D facial animation. Keller, M., et al. [51] constructed a dataset containing body surface-skeleton pairs extracted from 2000 X-ray absorptiometry (DXA) scans. A regressor was trained to infer the inside skeleton given the outside body surface of humans in various shapes and poses. In these examples, the input are the texts, audios and body surfaces, while the ground truth, a.k.a. annotations, are the corresponding videos, 3D facial models and skeletons. In [52], the authors constructed a paired pose-organ dataset and trained a deep model on it to infer the deformation of internal organs from patients' poses. The pose parameters were derived from whole-body skin segmentations of the CT dataset, while the organ deformations were calculated from the 3D models of the corresponding internal organs. In *MedShapeNet*, *pairedness* is defined as having two composites (anatomical shapes and/or meta information) coming from the same subject,

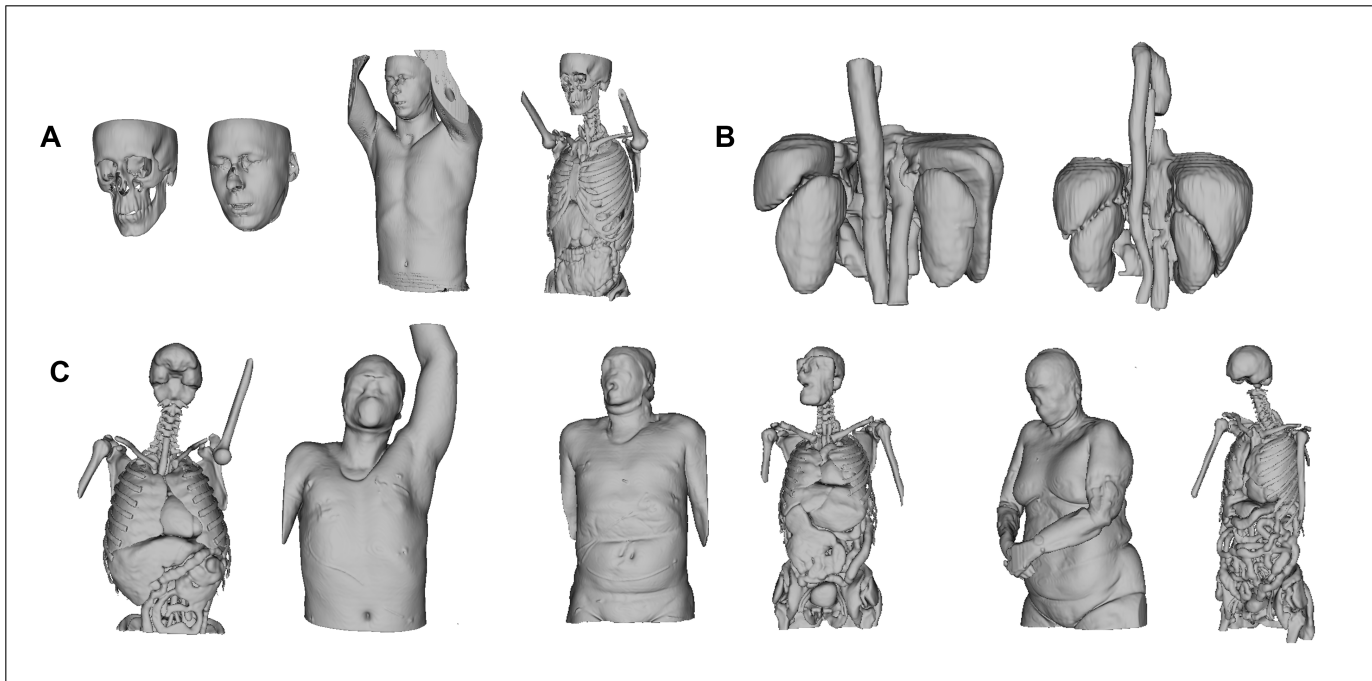


Fig. 5. Examples of paired anatomical shapes in *MedShapeNet*. (A) Paired skins, muscles, fat, different tissues, organs and bones derived from whole-body PET-CT segmentations. (B) Paired abdominal anatomies (from the FLAIR and AMOS challenges, respectively), including liver, spleen, pancreas, right kidney, left kidney, stomach, gallbladder, esophagus, aorta, inferior vena cava, right adrenal gland, left adrenal gland, and duodenum. (C) Paired internal anatomies and body surfaces derived from the *TotalSegmentor* dataset. Note: different anatomies have different labels in the segmentations. However, for illustration consistency, we use the same color (gray) for different anatomical shapes

TABLE 3  
A Non-inclusive List of Benchmarks Derived from *MedShapeNet*

Discriminative Benchmarks		Reconstructive Benchmarks		Variational Benchmarks	
input (shape)	ground truth (meta)	input (shape)	ground truth (shape)	input (shape)	ground truth (shape+meta)
liver	tumor	skull	face	face	face + age
kidney	tumor	ribs+spines	torso organs	face	face + AUD
brain	tumor	skin	body fat	face	face + CUD
brain	Alzheimer’s disease (AD)	full skeleton	skin	brain	brain + AD
brain	AUD				
brain	CUD				
face	CUD				
face	AUD				
face	age				
bain	age				
coronary artery	coronary artery disease (CAD)				
myocardium	infarction				
shapes	anatomical categories				

and one of them is used as input and the other is used as the ground truth. The most basic paired data in *MedShapeNet* consist of the shapes and their corresponding anatomical categories, such as ‘liver’, ‘heart’, ‘kidney’, and ‘lung’, which can be used to train a classifier for anatomical shape categorization. Synthetic shapes are marked with ‘\_synthetic’, to distinguish them from shapes obtained from real imaging data.

#### 4.1 Benchmarks Derived from *MedShapeNet*

Benchmark datasets for various interesting shape-based applications can be derived from *MedShapeNet* in the form of paired data, which facilitate supervised learning of a mapping relationship, i.e., paired data can be used as input and ground truth for training a deep neural network. Based on their direct applications, we roughly group all

potential benchmarks into three categories: *discriminative*, *reconstructive* and *variational*. The following discusses the three categories of benchmarks in detail. Table 3 shows a non-inclusive list of benchmarks (paired data) that can be derived from *MedShapeNet*. In Section 4.2, we present in specific four of the benchmarks and their corresponding use cases.

##### 4.1.1 Discriminative Benchmarks

The paired data are comprised of the patients’ meta information, such as pathologies, medical histories, and the corresponding anatomical shapes. An example of such paired data would be the liver shapes from healthy subjects and patients diagnosed with liver cancer. The health status (i.e., healthy, cancerous) is extracted from the patients’ meta information, while the live shapes

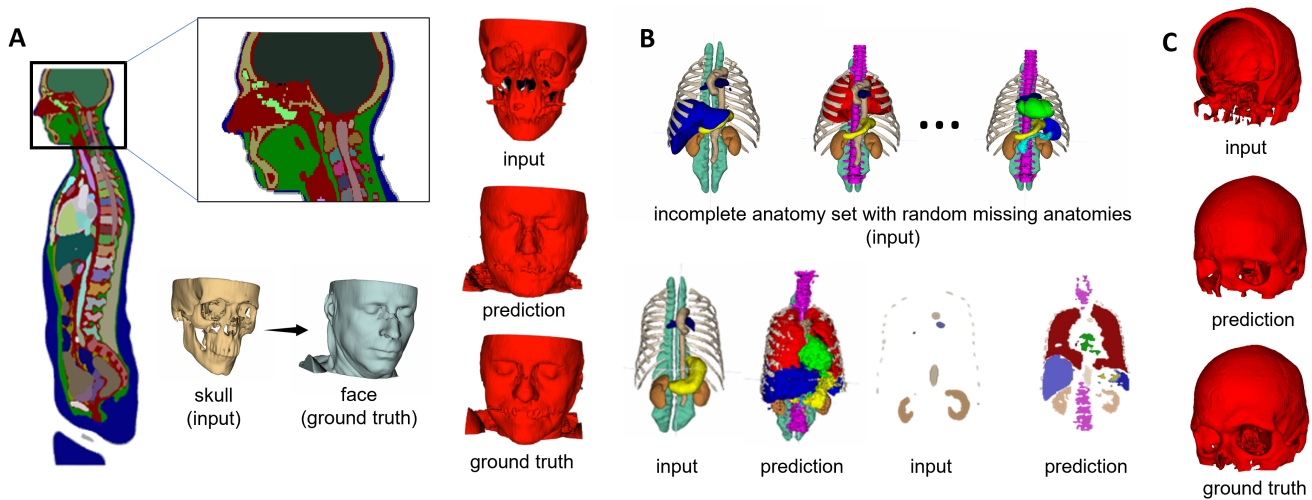


Fig. 6. Benchmarks for various vision applications can be derived from *MedShapeNet*, such as (A) forensic facial reconstruction, (B) anatomical shape reconstruction, and (C) skull reconstruction.

are derived from the corresponding segmentation masks. These benchmarks are mainly used for diagnostic tasks, in which a classifier is trained to discriminate cancerous livers from healthy ones based on liver shapes. Diagnosis (screening) of a pathological condition, such as cancer, is usually based on gray-scale medical images. Nevertheless, with the *Discriminative* benchmarks, one can investigate the possibility of discriminating between pathological and healthy subjects using only the shape of the affected organ(s). Furthermore, analogous to 3D shape classification for shape retrieval, a classifier can be trained to classify the shapes into different anatomical categories.

#### 4.1.2 Reconstructive Benchmarks

The paired data are comprised of different anatomical shapes derived from the whole-body segmentations of a patient. These benchmarks are usually used in reconstructive tasks, where the 3D shapes of an anatomy need to be reconstructed under the geometric constraint of existing ones. Numerous novel applications can be developed using such paired data. For example, given paired skull-face shapes (Figure 5), we can train a regressor to reconstruct human faces from the skeletal remains, specifically the skulls, to automate forensic facial reconstruction [145], which is considered a tedious, expensive and highly subjective procedure in archaeological research and criminal investigation; given paired skin-fat shapes derived from whole-body segmentations (Figure 5), a machine learning model can be trained to predict the spatial distribution of body fat, an important health risk indicator, from body surfaces (i.e., skins) [146]; similarly, we can also infer other internal body compositions (e.g., skeletons, organs) from a person’s body surface and vice versa, or infer the 3D shape a missing internal organ given its surrounding anatomies. New reconstructions are expected to be naturally aligned with given anatomies (i.e., the input). Such a naturalness criterion is automatically enforced by training on the paired data derived from the same subject. Therefore, these benchmarks are also

potentially useful for applications where *realism* is desired e.g., animation.

#### 4.1.3 Variational Benchmarks

*Variational benchmarks* are usually used for conditional reconstruction of 3D anatomical shapes. Besides the geometric constraints and the *naturalness* criterion mentioned above, new reconstructions are expected to have an additional attribute, such as age, gender and pathology, which can be extracted from the patients’ meta information as in the *Discriminative Benchmarks*. For example, it is possible to reconstruct multiple faces of different ages from the same skull, by including the meta information *age* as a supervising factor during training. Similarly, it is also possible to impose a pathological condition, such as tumor, on healthy anatomies or model the morphological changes of an anatomy during disease progression [147]. Variational auto-encoder (VAE) [148] and GANs are commonly used for such conditional reconstructive tasks.

## 4.2 Use Cases of *MedShapeNet*

In this section, we describe five real-world use cases of *MedShapeNet*, including (1) a forensic facial reconstructor, which reconstructs soft facial structures from the underlying skull; (2) an anatomy completer [149], which reconstructs the 3D shapes of anatomies that are missing in the input; (3) a skull reconstructor, which reconstructs the full skull structures when the skull is damaged, e.g., when (part of) the cranium or facial bones are missing; (4) a brain shape classifier that detects tumorous brains and (5) anatomy education in AR/MR. We show that problems (1-3) can be solved under a shape completion/inpainting framework, an active area of research in computer vision [150], [151], [152], [153], [154], where the complete set of anatomies, the 3D head models and the full skulls are regarded as the ground truth, while the incomplete anatomy set (in which one or several anatomies are missing), the skulls and the damaged skulls are the input, respectively. Convolutional neural

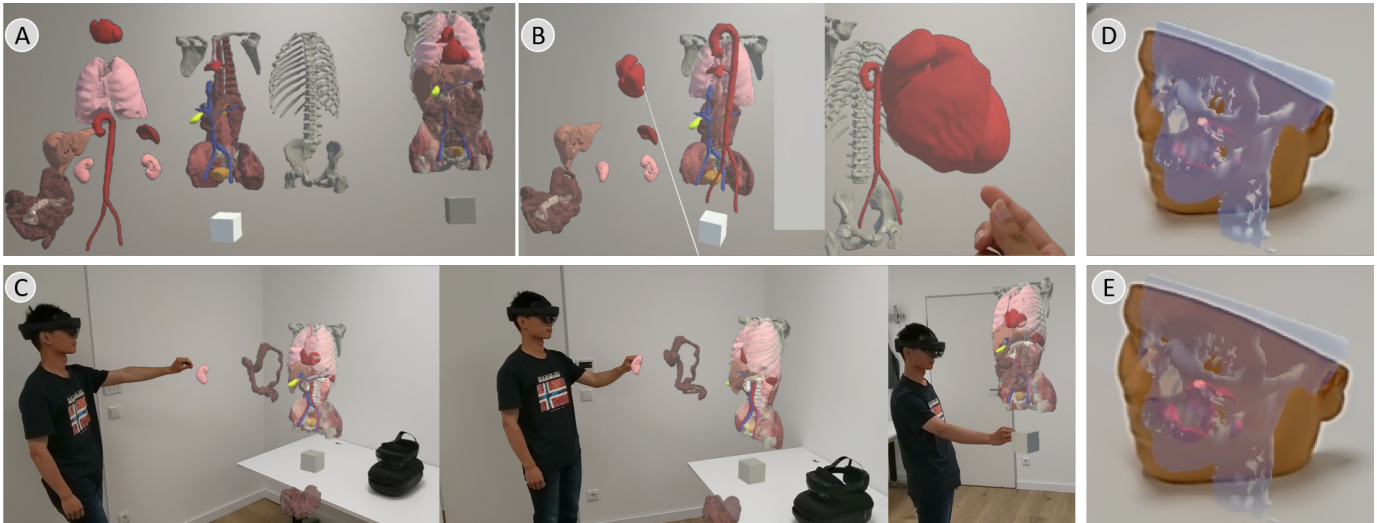


Fig. 7. A use case of *MedShapeNet* in AR-based anatomy education. (A) a whole-body model from *MedShapeNet* dissembled into individual anatomies. (B, C) anatomy manipulation in first- and third-person views. (D, E) a 3D-printed facial phantom and the corresponding skull and tumors.

networks are trained to learn the respective mappings. We derived such paired skull-face and anatomy datasets from whole body segmentations as described in Section 4. Damaged skulls can be generated by removing part of the bone structures from full skulls [24], [26]. Note that this section only aims at demonstrating how *MedShapeNet* can be used to solve vision/medical problems, rather than presenting SOTA results for each problem. To build upon the preliminary investigation, please refer to the codes and pretrained models that are publicly released at <https://github.com/Jianningli/medshapenet-feedback>.

#### 4.2.1 Forensic Facial Reconstruction

Forensic facial reconstruction refers to the process of restoring a person's facial features from the underlying skull. It is a common practice in archaeological research and criminal investigation, where the identity of an ancient person or victim needs to be determined from the remains [145]. Forensic facial reconstruction is usually carried out manually by a designer or sculptor, which is highly time-consuming and subjective. To automate this process, a facial reconstructor can be trained using paired skull-face data derived from the whole-body PET-CT segmentations in *MedShapeNet*, as seen in Figure 5. Figure 6 (A) shows how the paired skull-face data can be extracted from the whole-body segmentations in *MedShapeNet*. An input skull that is not including in training, the prediction from the facial reconstructor and the ground truth are also illustrated. We can see that the prediction and the ground truth bear sufficient resemblance for identification purposes.

#### 4.2.2 Multi-class Anatomy Completion

An anatomy completer learns the spatial and geometric relationship among different anatomies of the same person. Given a set of anatomies, the anatomy completer detects and then reconstructs the ones that are missing. Twelve organs are derived from the whole-body segmentations of TotalSegmentor, including the lung, heart, spleen, stomach, pancreas, spine, rib cage, liver, kidney, aorta, a pair of

autochthon muscles, and the pulmonary artery. Random anatomies are removed from them to create multiple incomplete anatomy sets, as shown in Figure 6 (B). A convolutional denoising auto-encoder is trained to learn a *many-to-one* mapping between the incomplete sets and the 12 anatomies. Figure 6 (B) also illustrates an input and the corresponding prediction in 3D and 2D coronary views. The completer reconstructs the 3D shapes of the missing anatomies in different classes, which geometrically and spatially fit existing ones. The multi-class anatomy completer is potentially helpful in creating pseudo labels for whole-body segmentation, where it generates initial segmentation masks for the anatomies that have not been annotated in a whole-body CT scan. Refer to [149] for implementation details of the anatomy completer.

#### 4.2.3 Skull Reconstruction

The task aims to reconstruct a full skull when the skull is damaged on the facial area, as seen in Figure 6 (C). Damaged skulls can be generated by erasing (part of) the facial voxels from full skulls, and a machine learning model can be trained on such paired skulls i.e., damaged and the corresponding full skull, to restore the erased voxels. Refer to [155] for implementation details of the skull reconstruction model. Damaged skulls can also be generated by erasing voxels around the cranium, and the same model can be trained for automatic cranial implant design [24], [26].

#### 4.2.4 Screening and Classification of Brain Tumors

Conventional data-driven methods for the screening and classification of brain tumors are usually based on grayscale MRIs [156], [157], [158]. The input of the classifier can be either the whole or skull-stripped MRI scans [159]. In this use case, we train a convolutional neural network (CNN)-based classifier using instead only the brain shapes represented as binary voxel grids, to discriminate between tumorous and healthy brains. The classifier has shown good convergence and generalizability, achieving over 80%

accuracy on the training and test set, respectively. The experiment demonstrates that the existence of tumors are reflected on the brain morphologies that can be captured by a standard CNN-based classifier, and that voxel features from gray-scale MRIs are redundant for the tumor detection task. Similar results are observed when the classifier is trained to distinguish brain shapes from male and females. It remains to be investigated whether the conclusion holds true for the stratification of different tumor subtypes.

Nevertheless, the classifier cannot converge properly when trained to discriminate brain shapes extracted from healthy subjects and CUD or AD patients, indicating that these brain pathologies are not well reflected on shape features. As discussed in Section 2, how to extract more discriminative shape features or incorporate voxel features into the training process when shape features alone are sufficient require future investigation.

#### 4.2.5 Anatomy Education in AR/MR & 3D Printing

Besides data-driven research, *MedShapeNet* can also benefit a variety of AR/MR applications that require 3D anatomical models [160]. A typical use case is AR-based anatomy education, which, different from conventional teaching methods, relies on virtual anatomical models [161]. In *MedShapeNet*, these 3D models are freely available to users and can be conveniently obtained using the online interface of *MedShapeNet* (to be discussed in Section 5). In Figure 7 (A), a whole-body model is displayed using the *Microsoft HoloLens* AR glasses. The whole-body model can be disassembled into individual anatomies, which can be moved, zoomed in/out and rotated and in the virtual environment, allowing students to learn the shape and relative position of an anatomical structure. Figure 7 (B) and Figure 7 (C) show the manipulation of the heart and the kidney in the first-person and third-person views, from the perspective of a teacher. Wherever necessary, these virtual models can also be converted into physical models via 3D printing. Figure 7 (D) and Figure 7 (E) show a 3D-printed facial phantom and a virtual skull model registered to the phantom. The virtual tumor models are also displayed on top of the registered models to show their relative position inside the skull of the patient.

### 4.3 Potential Negative Impact

To avoid potentially harmful societal impact, computer vision research involving human-derived data should be conducted with care. Since *MedShapeNet* is designed specifically for research at the junction of computer vision and medicine, proper ethics guidelines should be followed throughout methodology development and experimental design. For example, publicly sharing neuroimaging data bears high privacy risks and should be regulated, since they contain patients' facial profiles [162], [163]. A study shows that participants who are anonymously involved in a clinical trial can be identified by matching the faces reconstructed from their head MRI scans with photographs on social media, with the help of a face recognition software [113]. Therefore, besides removing patients' meta information before releasing neuroimaging data, defacing is also commonly practiced [164], [165]. Nevertheless, as

demonstrated by the forensic facial reconstruction example described in Section 4.2.1, the facial profiles of the patients can be reconstructed from skulls, where the entire facial structures are absent. Further removing the facial bones from skulls cannot completely resolve the issue either, as we have shown in our previous study that a machine learning model can reconstruct the original skulls even when the skulls are damaged (e.g., part of the bones on a skull are missing) [155], as seen in Figure 6 (C). Facial profiles can still be restored by first repairing the damaged skull using a skull reconstruction model discussed in Section 4.2.3 and then applying the facial reconstructor to the reconstructed skull, according to Figure 6 (C, A). *MedShapeNet* facilitates the training of face/skull reconstruction models for anyone with a basic command of machine learning, but at the same time makes it more difficult to protect patients' privacy when it comes to sharing neuroimaging data.

Another double-edged use case of *MedShapeNet* is to train a machine learning model to identify drug or alcohol consumption/addiction based on facial features. Users can easily retrieve the facial models of SUD and normal cohorts from *MedShapeNet* and train a binary classifier on them. The application benefits early detection and intervention of SUD, but may be abused for discrimination in unauthorized situations. Furthermore, since *MedShapeNet* preserves the correspondence between the shapes and the source datasets, patients' meta information, such as age, race, gender, medical history, etc., if available in the source datasets, can be mapped to each shape model, which facilitates the learning of some controversial mapping relationships. For example, the ethnic identity or medical history could potentially be predicted based on a person's skull or facial profiles by training a classifier.

It is therefore the responsibility of the researchers to weigh the social benefits against the potential negative societal impacts while developing models using *MedShapeNet*.

## 5 A WEB INTERFACE FOR *MedShapeNet*

A user-friendly, easy-to-use web API facilitates convenient access to the shape data within *MedShapeNet*, and makes it easier for researchers to use the database in their research. Inspired by the web API of the well-known *ShapeNet* (<https://shapenet.org/>), we developed a web-based interface for *MedShapeNet*, which can be visited at <https://medshapenet-ikim.streamlit.app/>. Users can search, download and inspect in a 3D viewer an individual shape, or batch download an entire category of anatomies. Desired shapes can be retrieved by the corresponding anatomy classes, such as 'heart', 'brain', 'hip', 'liver', as shown in Figure 8 (A, C). The names of the shapes matching the search query will be displayed in a drop-down menu. The corresponding shape will be displayed in a 3D viewer underneath the search box after clicking on one of the search results (Figure 8 (B)). An overview of currently available medical shapes, their categories and download links is also shown on the main page of the interface (Figure 8 (E)). The size of the overall database amounts to several terabytes (TB), which substantially exceeds the free space quota of most server providers, including *Streamlit*. We solve the

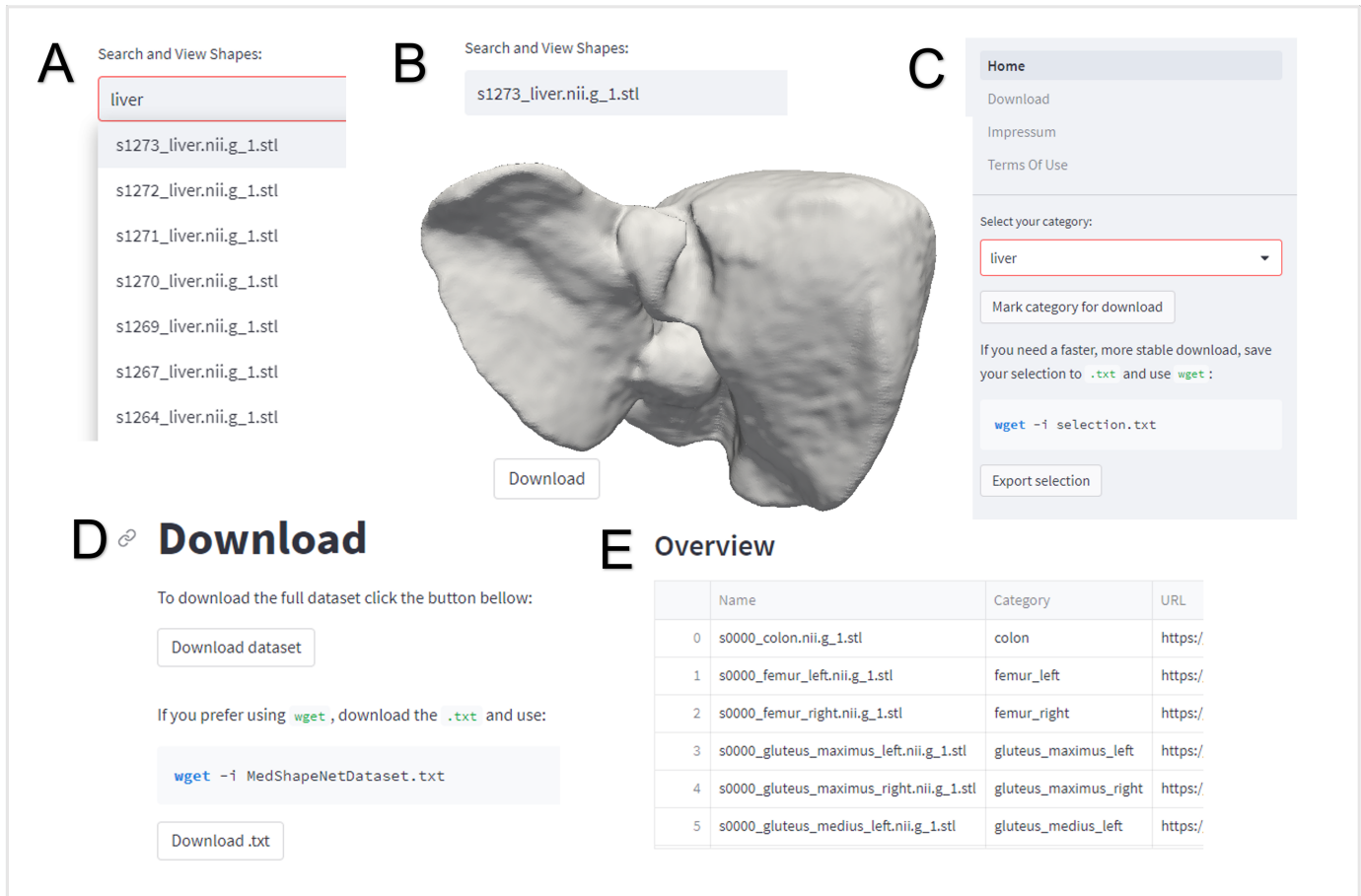


Fig. 8. Main panels of the *MedShapeNet* web interface. A, C: choosing an anatomy category 'liver'. B: selecting an anatomy instance 's12273\_liver.nii.g\_1.stl' and displaying it in an interactive 3D viewer. D: downloading the entire *MedShapeNet* database. E: an overview of currently available medical shapes, their categories and download links.

TABLE 4  
Valid Search Queries for the *MedShapeNet* Web Interface

CT	mri	brain	skull	brain	vertebrae	stomach
bladder	bowel	rib	sacrum	bowel	scapula	lung
heart	ventricle	atrium	kidney	iliopsoas	iliac	artery
gland	gluteus	femur	esophagus	autochthon	colon	aorta
trachea	hip	pancreas	vein	bowel	clavicula	myocardium
humerus	vena_cava	duodenum	face	vessel_tree	glioblastoma	cranial_defect

problem by separating the shape storage (*sciebo*) from the *Streamlit* server running the web interface, to reduce the cost of storing large quantities of data on servers.

### 5.1 Search Queries

The *MedShapeNet* web interface returns shapes of choice by matching users' queries with the anatomy classes provided in the names of the shape files. Table 4 shows a list of possible queries that will return at least one result in the *MedShapeNet* web interface. The search query for anatomies whose names contain multiple words is composed of the individual words and underscores that connect the words (e.g., atrium\_left, gluteus\_medius\_left, inferior\_vena\_cava, lung\_upper\_lobe). No results will be displayed if the search query does not match any existing file names. Users can search by anatomy (e.g., liver) or pathology (e.g., tumor).

### 5.2 User Feedback

We use GitHub to manage the communication among users, developers, and contributors of *MedShapeNet*. It provides a mechanism for researchers to contribute shapes, provide feedbacks (e.g., report corrupted shapes, suggest improvements) and showcase their own research/applications utilizing *MedShapeNet*. As an incentive, shape contributors can be credited as collaborators of the *MedShapeNet* project and their research can be featured on the GitHub page upon request. Detailed contribution guidelines is available at <https://github.com/Jianningli/medshapenet-feedback>. A quality check will be performed before incorporating new shapes into *MedShapeNet*, to avoid introducing corrupted data. Since the shape data come from different sources, a consistency check will also be conducted to ensure that the

shape data with the same class annotations correspond to the exact same anatomical part.

## 6 DISCUSSION AND CONCLUSION

High-quality, annotated datasets are valuable assets for data-driven research. We created *MedShapeNet*, with the firm belief that, in the near future, it will become a commonly referenced resource in the computer vision and medical imaging community. The construction of *MedShapeNet* is an ongoing effort and requires continuous contributions from the community, since the majority of its shape collections are acquired from data sources not owned by us. *MedShapeNet* also relies on the community to refine its shape collection and define more interesting use cases at the junction of computer vision and medical imaging (refer to Section 5.2). In this white paper, we have introduced the initial efforts we have taken to construct *MedShapeNet*, most importantly by (1) bringing together the community for data contribution (most of the co-authors have contributed a source dataset for the shape collection); (2) deriving benchmark datasets for several interesting applications (Section 4.2), and open-sourcing them to support future research on the respective directions; (3) constructing an online interface to facilitate searching and downloading shapes of choice (Section 5); and (4) bringing up several interesting shape-related research topics that are worthy of future investigation (Section 2) and discussing the precautions that should be taken to comply with the ethics guidelines (Section 4.3). Furthermore, compared to vision datasets, large medical datasets are much more difficult to curate due to the sensitive, distributed and scarce nature of medical images. As a result, the medical imaging community has only recently started catching up with the development of vision algorithms that can exploit large datasets, with more and more medical researchers becoming open to data-sharing in recent years. Thus, *MedShapeNet* has the potential to bridge the gap between the vision and medical imaging community, by providing a versatile dataset that both vision and medical researchers are accustomed to. Last but not least, *MedShapeNet* is a freely available 3D repository for extended reality research and applications. For future development of *MedShapeNet*, we will primarily focus on the following aspects:

- **Increase the size and diversity of the shape collection:** we will collect more shapes, especially pathological ones (e.g., glioblastoma, aorta with aneurysm) to further enrich *MedShapeNet*, and engage more researchers from the community to join the initiative.
- **Promote *MedShapeNet*:** we will disseminate *MedShapeNet* more actively in the research community of computer vision and medical imaging, by presenting it in conferences, symposia, seminars and classrooms (teaching), and organizing hackweeks/workshops/challenges.
- **Define new benchmarks and establish more use cases:** we, together with the community, will derive more benchmark datasets from *MedShapeNet* and explore interesting use cases based on them.
- **Improve the shape search portal:** we will improve the online portal of *MedShapeNet* by iteratively refining the shape search functionality and improving the user interface for a better user experience.
- **Provide more shape annotations:** we will extract more meta information from the source datasets and incorporate them into the corresponding shape data as annotations.
- **Redesign the naming convention of the shapes:** we will design a more inclusive and compact naming convention for the shapes, from which essential information, such as anatomy categories, source datasets, pathologies, etc., can be deduced.

## ACKNOWLEDGMENTS

This work was supported by the REACT-EU project KITE (Plattform für KI-Translation Essen, EFRE-0801977, <https://kite.ikim.nrw/>), FWF enFaced 2.0 (KLI 1044, <https://enfaced2.ikim.nrw/>) and AutoImplant (<https://autoimplant.ikim.nrw/>). Behrus Puladi was funded by the Medical Faculty of RWTH Aachen University as part of the Clinician Scientist Program. In addition, we acknowledge the National Natural Science Foundation of China (81971709; M-0019; 82011530141). The work of J. Chen was supported by the Bundesministerium für Bildung und Forschung (BMBF, Ref. 161L0272). The work of ISAS was supported by the “Ministerium für Kultur und Wissenschaft des Landes Nordrhein-Westfalen” and “Der Regierende Bürgermeister von Berlin, Senatskanzlei Wissenschaft und Forschung”. Furthermore, we acknowledge the *Center for Virtual and Extended Reality in Medicine* (ZvRM, <https://zvrm.ume.de/>) of the University Hospital Essen. The CT-ORG dataset was obtained from the Cancer Imaging Archive (TCIA). CT-ORG was supported in part by grants from the National Cancer Institute, 1U01CA190214 and 1U01CA187947. We thank all those who have contributed to the *MedShapeNet* collection (directly or indirectly).

## REFERENCES

- [1] D. Shen, G. Wu, and H.-I. Suk, “Deep learning in medical image analysis,” *Annual review of biomedical engineering*, vol. 19, pp. 221–248, 2017.
- [2] J. Egger, C. Gsaxner, A. Pepe, K. L. Pomykala, F. Jonske, M. Kurz, J. Li, and J. Kleesiek, “Medical deep learning—a systematic meta-review,” *Computer Methods and Programs in Biomedicine*, vol. 221, p. 106874, 2022.
- [3] J. Egger, A. Pepe, C. Gsaxner, Y. Jin, J. Li, and R. Kern, “Deep learning—a first meta-survey of selected reviews across scientific disciplines, their commonalities, challenges and research impact,” *PeerJ Computer Science*, vol. 7, p. e773, 2021.
- [4] C. Sun, A. Shrivastava, S. Singh, and A. Gupta, “Revisiting unreasonable effectiveness of data in deep learning era,” in *Proceedings of the IEEE international conference on computer vision*, 2017, pp. 843–852.
- [5] J. Deng, W. Dong, R. Socher, L.-J. Li, K. Li, and L. Fei-Fei, “Imagenet: A large-scale hierarchical image database,” in *2009 IEEE conference on computer vision and pattern recognition*. Ieee, 2009, pp. 248–255.
- [6] A. Krizhevsky, G. Hinton *et al.*, “Learning multiple layers of features from tiny images,” 2009.

- [7] J. Geyer, Y. Kassahun, M. Mahmudi, X. Ricou, R. Durgesh, A. S. Chung, L. Hauswald, V. H. Pham, M. Mühlegg, S. Dorn, T. Fernandez, M. Jänicke, S. Mirashi, C. Savani, M. Sturm, O. Vorobiov, M. Oelker, S. Garreis, and P. Schuberth, "A2D2: Audi Autonomous Driving Dataset," 2020. [Online]. Available: <https://www.a2d2.audi>
- [8] Z. Wu, S. Song, A. Khosla, F. Yu, L. Zhang, X. Tang, and J. Xiao, "3d shapenets: A deep representation for volumetric shapes," in *Proceedings of the IEEE conference on computer vision and pattern recognition*, 2015, pp. 1912–1920.
- [9] A. X. Chang, T. Funkhouser, L. Guibas, P. Hanrahan, Q. Huang, Z. Li, S. Savarese, M. Savva, S. Song, H. Su *et al.*, "Shapenet: An information-rich 3d model repository," *arXiv preprint arXiv:1512.03012*, 2015.
- [10] M.-X. Lin, J. Yang, H. Wang, Y.-K. Lai, R. Jia, B. Zhao, and L. Gao, "Single image 3d shape retrieval via cross-modal instance and category contrastive learning," in *Proceedings of the IEEE/CVF International Conference on Computer Vision*, 2021, pp. 11 405–11 415.
- [11] M. Savva, F. Yu, H. Su, M. Aono, B. Chen, D. Cohen-Or, W. Deng, H. Su, S. Bai, X. Bai *et al.*, "Shrec16 track: largescale 3d shape retrieval from shapenet core55," in *Proceedings of the eurographics workshop on 3D object retrieval*, vol. 10, 2016.
- [12] X. Liu, Z. Han, Y.-S. Liu, and M. Zwicker, "Fine-grained 3d shape classification with hierarchical part-view attention," *IEEE Transactions on Image Processing*, vol. 30, pp. 1744–1758, 2021.
- [13] Y. Zhang, J. Lin, C. He, Y. Chen, K. Jia, and L. Zhang, "Masked surfel prediction for self-supervised point cloud learning," *arXiv preprint arXiv:2207.03111*, 2022.
- [14] X. Yan, L. Lin, N. J. Mitra, D. Lischinski, D. Cohen-Or, and H. Huang, "Shapeformer: Transformer-based shape completion via sparse representation," in *Proceedings of the IEEE/CVF Conference on Computer Vision and Pattern Recognition*, 2022, pp. 6239–6249.
- [15] J. Wang, J. Lin, Q. Yu, R. Liu, Y. Chen, and S. X. Yu, "3d shape reconstruction from free-hand sketches," in *European Conference on Computer Vision*. Springer, 2022, pp. 184–202.
- [16] L. Yi, L. Shao, M. Savva, H. Huang, Y. Zhou, Q. Wang, B. Graham, M. Engelcke, R. Klokov, V. Lempitsky *et al.*, "Large-scale 3d shape reconstruction and segmentation from shapenet core55," *arXiv preprint arXiv:1710.06104*, 2017.
- [17] I. Sarasua, S. Pölsterl, and C. Wachinger, "Hippocampal representations for deep learning on alzheimer's disease," *Scientific reports*, vol. 12, no. 1, p. 8619, 2022.
- [18] M. Rezanejad, M. Khodadad, H. Mahyar, H. Lombaert, M. Gruninger, D. Walther, and K. Siddiqi, "Medial spectral coordinates for 3d shape analysis," in *Proceedings of the IEEE/CVF Conference on Computer Vision and Pattern Recognition*, 2022, pp. 2686–2696.
- [19] T. Ringwald and R. Stiefelhagen, "Adaptiope: A modern benchmark for unsupervised domain adaptation," in *Proceedings of the IEEE/CVF Winter Conference on Applications of Computer Vision*, 2021, pp. 101–110.
- [20] O. Kodym, M. Španěl, and A. Herout, "Deep learning for cranioplasty in clinical practice: Going from synthetic to real patient data," *Computers in Biology and Medicine*, vol. 137, p. 104766, 2021.
- [21] A. Morais, J. Egger, and V. Alves, "Automated computer-aided design of cranial implants using a deep volumetric convolutional denoising autoencoder," in *World conference on information systems and technologies*. Springer, 2019, pp. 151–160.
- [22] F. Matzkin, V. Newcombe, S. Stevenson, A. Khetani, T. Newman, R. Digby, A. Stevens, B. Glocker, and E. Ferrante, "Self-supervised skull reconstruction in brain ct images with decompressive craniectomy," in *Medical Image Computing and Computer Assisted Intervention—MICCAI 2020: 23rd International Conference, Lima, Peru, October 4–8, 2020, Proceedings, Part II 23*. Springer, 2020, pp. 390–399.
- [23] O. Kodym, M. Španěl, and A. Herout, "Cranial defect reconstruction using cascaded cnn with alignment," in *Towards the Automatization of Cranial Implant Design in Cranioplasty: First Challenge, AutoImplant 2020, Held in Conjunction with MICCAI 2020, Lima, Peru, October 8, 2020, Proceedings 1*. Springer, 2020, pp. 56–64.
- [24] J. Li, P. Pimentel, A. Szengel, M. Ehlke, H. Lamecker, S. Zachow, L. Estacio, C. Doenitz, H. Ramm, H. Shi *et al.*, "Autoimplant 2020-first miccai challenge on automatic cranial implant design," *IEEE transactions on medical imaging*, vol. 40, no. 9, pp. 2329–2342, 2021.
- [25] J. Li, G. von Campe, A. Pepe, C. Gsaxner, E. Wang, X. Chen, U. Zefferer, M. Tödtling, M. Krall, H. Deutschmann *et al.*, "Automatic skull defect restoration and cranial implant generation for cranioplasty," *Medical Image Analysis*, vol. 73, p. 102171, 2021.
- [26] J. Li, D. G. Ellis, O. Kodym, L. Rauschenbach, C. Rieß, U. Sure, K. H. Wrede, C. M. Alvarez, M. Wodzinski, M. Daniol *et al.*, "Towards clinical applicability and computational efficiency in automatic cranial implant design: An overview of the autoimplant 2021 cranial implant design challenge," *Medical Image Analysis*, p. 102865, 2023.
- [27] A. Dai, C. Ruizhongtai Qi, and M. Nießner, "Shape completion using 3d-encoder-predictor cnns and shape synthesis," in *Proceedings of the IEEE conference on computer vision and pattern recognition*, 2017, pp. 5868–5877.
- [28] X. Han, Z. Li, H. Huang, E. Kalogerakis, and Y. Yu, "High-resolution shape completion using deep neural networks for global structure and local geometry inference," in *Proceedings of the IEEE international conference on computer vision*, 2017, pp. 85–93.
- [29] J. Varley, C. DeChant, A. Richardson, J. Ruales, and P. Allen, "Shape completion enabled robotic grasping," in *2017 IEEE/RSJ international conference on intelligent robots and systems (IROS)*. IEEE, 2017, pp. 2442–2447.
- [30] D. Stutz and A. Geiger, "Learning 3d shape completion from laser scan data with weak supervision," in *Proceedings of the IEEE Conference on Computer Vision and Pattern Recognition*, 2018, pp. 1955–1964.
- [31] X. Wang, M. H. Ang, and G. H. Lee, "Voxel-based network for shape completion by leveraging edge generation," in *Proceedings of the IEEE/CVF international conference on computer vision*, 2021, pp. 13 189–13 198.
- [32] T. Heimann and H.-P. Meinzer, "Statistical shape models for 3d medical image segmentation: a review," *Medical image analysis*, vol. 13, no. 4, pp. 543–563, 2009.
- [33] A. Raju, S. Miao, D. Jin, L. Lu, J. Huang, and A. P. Harrison, "Deep implicit statistical shape models for 3d medical image delineation," in *proceedings of the AAAI conference on artificial intelligence*, vol. 36, no. 2, 2022, pp. 2135–2143.
- [34] E. O'Sullivan, L. S. van de Lande, A.-J. C. Oosting, A. Papaioannou, N. O. Jeelani, M. J. Koudstaal, R. H. Khonsari, D. J. Dunaway, S. Zafeiriou, and S. Schievano, "The 3d skull 0–4 years: A validated, generative, statistical shape model," *Bone reports*, vol. 15, p. 101154, 2021.
- [35] L. Luo, M. Wang, Y. Tian, F. Duan, Z. Wu, M. Zhou, and Y. Rozenholc, "Automatic sex determination of skulls based on a statistical shape model," *Computational and mathematical methods in medicine*, vol. 2013, 2013.
- [36] P. Pimentel, A. Szengel, M. Ehlke, H. Lamecker, S. Zachow, L. Estacio, C. Doenitz, and H. Ramm, "Automated virtual reconstruction of large skull defects using statistical shape models and generative adversarial networks," in *Cranial implant design challenge*. Springer, 2020, pp. 16–27.
- [37] M. A. Fuessinger, S. Schwarz, C.-P. Cornelius, M. C. Metzger, E. Ellis, F. Probst, W. Semper-Hogg, M. Gass, and S. Schlager, "Planning of skull reconstruction based on a statistical shape model combined with geometric morphometrics," *International journal of computer assisted radiology and surgery*, vol. 13, no. 4, pp. 519–529, 2018.
- [38] F. Cosentino, G. M. Raffa, G. Gentile, V. Agnese, D. Bellavia, M. Pilato, and S. Pasta, "Statistical shape analysis of ascending thoracic aortic aneurysm: correlation between shape and biomechanical descriptors," *Journal of Personalized Medicine*, vol. 10, no. 2, p. 28, 2020.
- [39] L. Gundelwein, H. Ramm, L. Goubergrits, M. Kelm, and H. Lamecker, "3d shape analysis for coarctation of the aorta," in *International workshop on shape in medical imaging*. Springer, 2018, pp. 73–77.
- [40] W. A. van Veldhuizen, R. C. Schuurmann, F. F. Ijpma, R. H. Kropman, G. A. Antoniou, J. M. Wolterink, and J.-P. P. de Vries, "A statistical shape model of the morphological variation of the infrarenal abdominal aortic aneurysm neck," *Journal of Clinical Medicine*, vol. 11, no. 6, p. 1687, 2022.
- [41] L. Petrelli, A. Pepe, A. Disanto, C. Gsaxner, J. Li, Y. Jin, D. Buongiorno, A. Brunetti, V. Bevilacqua, and J. Egger, "Geometric modeling of aortic dissections through convolution



- surfaces," in *Medical Imaging 2022: Imaging Informatics for Healthcare, Research, and Applications*, vol. 12037. SPIE, 2022, pp. 198–206.
- [42] A. V. Dalca, J. Guttag, and M. R. Sabuncu, "Anatomical priors in convolutional networks for unsupervised biomedical segmentation," in *Proceedings of the IEEE Conference on Computer Vision and Pattern Recognition*, 2018, pp. 9290–9299.
- [43] W. Lin, H. Liu, L. Gu, and Z. Gao, "A geometry-constrained deformable attention network for aortic segmentation," in *Medical Image Computing and Computer Assisted Intervention–MICCAI 2022: 25th International Conference, Singapore, September 18–22, 2022, Proceedings, Part V*. Springer, 2022, pp. 287–296.
- [44] F. Williams, T. Schneider, C. Silva, D. Zorin, J. Bruna, and D. Panozzo, "Deep geometric prior for surface reconstruction," in *Proceedings of the IEEE/CVF Conference on Computer Vision and Pattern Recognition*, 2019, pp. 10 130–10 139.
- [45] J. Lötjönen, I. E. Magnin, L. Reinhardt, J. Nenonen, and T. Katila, "Automatic reconstruction of 3d geometry using projections and a geometric prior model," in *Medical Image Computing and Computer-Assisted Intervention–MICCAI'99: Second International Conference, Cambridge, UK, September 19–22, 1999. Proceedings 2*. Springer, 1999, pp. 192–201.
- [46] T. Zhao, K. Cao, J. Yao, I. Noguees, L. Lu, L. Huang, J. Xiao, Z. Yin, and L. Zhang, "3d graph anatomy geometry-integrated network for pancreatic mass segmentation, diagnosis, and quantitative patient management," in *Proceedings of the IEEE/CVF conference on computer vision and pattern recognition*, 2021, pp. 13 743–13 752.
- [47] F. Matzkin, V. Newcombe, B. Glocker, and E. Ferrante, "Cranial implant design via virtual craniectomy with shape priors," in *Towards the Automatization of Cranial Implant Design in Cranioplasty: First Challenge, AutoImplant 2020, Held in Conjunction with MICCAI 2020, Lima, Peru, October 8, 2020, Proceedings 1*. Springer, 2020, pp. 37–46.
- [48] B. Graham and L. Van der Maaten, "Submanifold sparse convolutional networks," *arXiv preprint arXiv:1706.01307*, 2017.
- [49] F. Yin, Y. Zhang, X. Wang, T. Wang, X. Li, Y. Gong, Y. Fan, X. Cun, Y. Shan, C. Oztireli *et al.*, "3d gan inversion with facial symmetry prior," in *Proceedings of the IEEE/CVF Conference on Computer Vision and Pattern Recognition*, 2023, pp. 342–351.
- [50] K. Kania, S. J. Garbin, A. Tagliasacchi, V. Estellers, K. M. Yi, J. Valentin, T. Trzciński, and M. Kowalski, "Blendfields: Few-shot example-driven facial modeling," in *Proceedings of the IEEE/CVF Conference on Computer Vision and Pattern Recognition*, 2023, pp. 404–415.
- [51] M. Keller, S. Zuffi, M. J. Black, and S. Pujades, "Osso: Obtaining skeletal shape from outside," in *Proceedings of the IEEE/CVF Conference on Computer Vision and Pattern Recognition*, 2022, pp. 20 492–20 501.
- [52] H. Guo, B. Planche, M. Zheng, S. Karanam, T. Chen, and Z. Wu, "Smpl-a: Modeling person-specific deformable anatomy," in *Proceedings of the IEEE/CVF Conference on Computer Vision and Pattern Recognition*, 2022, pp. 20 814–20 823.
- [53] D. Zhang, F. Huang, M. Khansari, T. T. Berendschot, X. Xu, B. Dashtbozorg, Y. Sun, J. Zhang, and T. Tan, "Automatic corneal nerve fiber segmentation and geometric biomarker quantification," *The European Physical Journal Plus*, vol. 135, no. 2, p. 266, 2020.
- [54] L. V. van Dijk, C. L. Brouwer, H. P. van der Laan, J. G. Burgerhof, J. A. Langendijk, R. J. Steenbakkers, and N. M. Sijtsema, "Geometric image biomarker changes of the parotid gland are associated with late xerostomia," *International Journal of Radiation Oncology\* Biology\* Physics*, vol. 99, no. 5, pp. 1101–1110, 2017.
- [55] C. Gsaxner, J. Li, A. Pepe, D. Schmalstieg, and J. Egger, "Inside-out instrument tracking for surgical navigation in augmented reality," in *Proceedings of the 27th ACM Symposium on Virtual Reality Software and Technology*, 2021, pp. 1–11.
- [56] M. Wodzinski, M. Daniol, M. Socha, D. Hemmerling, M. Stanuch, and A. Skalski, "Deep learning-based framework for automatic cranial defect reconstruction and implant modeling," *Computer Methods and Programs in Biomedicine*, vol. 226, p. 107173, 2022.
- [57] H. Akbari, L. Macyszyn, X. Da, M. Bilello, R. L. Wolf, M. Martinez-Lage, G. Biros, M. Alonso-Basanta, D. M. O'Rourke, and C. Davatzikos, "Imaging surrogates of infiltration obtained via multiparametric imaging pattern analysis predict subsequent location of recurrence of glioblastoma," *Neurosurgery*, vol. 78, no. 4, p. 572, 2016.
- [58] F. Seker-Polat, N. Pinarbasi Degirmenci, I. Solaroglu, and T. Bagci-Onder, "Tumor cell infiltration into the brain in glioblastoma: from mechanisms to clinical perspectives," *Cancers*, vol. 14, no. 2, p. 443, 2022.
- [59] E. J. Limkin, S. Reuzé, A. Carré, R. Sun, A. Schernberg, A. Alexis, E. Deutsch, C. Féré, and C. Robert, "The complexity of tumor shape, spiculatedness, correlates with tumor radiomic shape features," *Scientific reports*, vol. 9, no. 1, p. 4329, 2019.
- [60] J. Wasserthal, H.-C. Breit, M. T. Meyer, M. Pradella, D. Hinck, A. W. Sauter, T. Heye, D. Boll, J. Cyriac, S. Yang *et al.*, "Totalsegmentator: robust segmentation of 104 anatomical structures in ct images," *Radiology: Artificial Intelligence*, vol. 5, 2023.
- [61] J. Li, M. Krall, F. Trummer, A. R. Memon, A. Pepe, C. Gsaxner, Y. Jin, X. Chen, H. Deutschmann, U. Zefferer *et al.*, "Mug500+: Database of 500 high-resolution healthy human skulls and 29 craniotomy skulls and implants," *Data in Brief*, vol. 39, p. 107524, 2021.
- [62] J. S. Elam, M. F. Glasser, M. P. Harms, S. N. Sotiropoulos, J. L. Andersson, G. C. Burgess, S. W. Curtiss, R. Oostenveld, L. J. Larson-Prior, J.-M. Schoffelen *et al.*, "The human connectome project: a retrospective," *NeuroImage*, vol. 244, p. 118543, 2021.
- [63] C. Gsaxner, J. Wallner, X. Chen, W. Zemann, and J. Egger, "Facial model collection for medical augmented reality in oncologic cranio-maxillofacial surgery," *Scientific data*, vol. 6, no. 1, pp. 1–7, 2019.
- [64] L. Radl, Y. Jin, A. Pepe, J. Li, C. Gsaxner, F.-h. Zhao, and J. Egger, "AvT: Multicenter aortic vessel tree cta dataset collection with ground truth segmentation masks," *Data in Brief*, vol. 40, p. 107801, 2022.
- [65] L. Lindner, D. Wild, M. Weber, M. Kolodziej, G. von Campe, and J. Egger, "Skull-stripped mri gbm datasets (and segmentations)," 6 2019.
- [66] O. Kodym, J. Li, A. Pepe, C. Gsaxner, S. Chilamkurthy, J. Egger, and M. Španěl, "Skullbreak/skullfix-dataset for automatic cranial implant design and a benchmark for volumetric shape learning tasks," *Data in Brief*, vol. 35, p. 106902, 2021.
- [67] A. Sekuboyina, M. Rempfler, A. Valentinitich, B. H. Menze, and J. S. Kirschke, "Labeling vertebrae with two-dimensional reformations of multidetector ct images: an adversarial approach for incorporating prior knowledge of spine anatomy," *Radiology: Artificial Intelligence*, vol. 2, no. 2, p. e190074, 2020.
- [68] N. Heller, F. Isensee, K. H. Maier-Hein, X. Hou, C. Xie, F. Li, Y. Nan, G. Mu, Z. Lin, M. Han *et al.*, "The state of the art in kidney and kidney tumor segmentation in contrast-enhanced ct imaging: Results of the kits19 challenge," *Medical Image Analysis*, p. 101821, 2020.
- [69] U. Baid, S. Ghodasara, S. Mohan, M. Bilello, E. Calabrese, E. Colak, K. Farahani, J. Kalpathy-Cramer, F. C. Kitamura, S. Pati *et al.*, "The rsna-asnr-miccai brats 2021 benchmark on brain tumor segmentation and radiogenomic classification," *arXiv preprint arXiv:2107.02314*, 2021.
- [70] B. H. Menze, A. Jakab, S. Bauer, J. Kalpathy-Cramer, K. Farahani, J. Kirby, Y. Burren, N. Porz, J. Slotboom, R. Wiest *et al.*, "The multimodal brain tumor image segmentation benchmark (brats)," *IEEE transactions on medical imaging*, vol. 34, no. 10, pp. 1993–2024, 2014.
- [71] S. Bakas, H. Akbari, A. Sotiras, M. Bilello, M. Rozycki, J. S. Kirby, J. B. Freymann, K. Farahani, and C. Davatzikos, "Advancing the cancer genome atlas glioma mri collections with expert segmentation labels and radiomic features," *Scientific data*, vol. 4, no. 1, pp. 1–13, 2017.
- [72] A. Ben-Hamadou, O. Smaoui, A. Rekik, S. Pujades, E. Boyer, H. Lim, M. Kim, M. Lee, M. Chung, Y.-G. Shin, M. Leclercq, L. Cevindanes, J. C. Prieto, S. Zhuang, G. Wei, Z. Cui, Y. Zhou, T. Dascalu, B. Ibragimov, T.-H. Yong, H.-G. Ahn, W. Kim, J.-H. Han, B. Choi, N. van Nistelrooij, S. Kempers, S. Vinayahalingam, J. Strippoli, A. Thollot, H. Setbon, C. Trosset, and E. Ladroit, "3dteethseg22: 3d teeth scan segmentation and labeling challenge," *arXiv preprint arXiv:2305.18277*, 2023.
- [73] A. Ben-Hamadou, O. Smaoui, H. Chaabouni-Chouayakh, A. Rekik, S. Pujades, E. Boyer, J. Strippoli, A. Thollot, H. Setbon, C. Trosset *et al.*, "Teeth3ds: a benchmark for teeth segmentation and labeling from intra-oral 3d scans," *arXiv preprint arXiv:2210.06094*, 2022.
- [74] V. Andrearczyk, V. Oreiller, M. Abobakr, A. Akhavanallaf, P. Balermipas, S. Boughdad, L. Capriotti, J. Castelli, C. Cheze

- Le Rest, P. Decazes, R. Correia *et al.*, "Overview of the HECKTOR challenge at MICCAI 2022: Automatic head and neck tumor segmentation and outcome prediction in PET/CT," in *Head and Neck Tumor Segmentation and Outcome Prediction*. Springer, 2022, pp. 1–30.
- [75] V. Oreiller, V. Andrearczyk, M. Jreige, S. Boughdad, H. Elhalawani, J. Castelli, M. Vallieres, S. Zhu, J. Xie, Y. Peng *et al.*, "Head and neck tumor segmentation in pet/ct: the hecktor challenge," *Medical image analysis*, vol. 77, p. 102336, 2022.
- [76] J. Shapey, A. Kujawa, R. Dorent, G. Wang, A. Dimitriadis, D. Grishchuk, I. Paddick, N. Kitchen, R. Bradford, S. R. Saeed *et al.*, "Segmentation of vestibular schwannoma from mri, an open annotated dataset and baseline algorithm," *Scientific Data*, vol. 8, no. 1, p. 286, 2021.
- [77] R. Dorent, A. Kujawa, M. Ivory, S. Bakas, N. Rieke, S. Joutard, B. Glocker, J. Cardoso, M. Modat, K. Batmanghelich *et al.*, "Crossmoda 2021 challenge: Benchmark of cross-modality domain adaptation techniques for vestibular schwannoma and cochlea segmentation," *Medical Image Analysis*, vol. 83, p. 102628, 2023.
- [78] P. Bilic, P. Christ, H. B. Li, E. Vorontsov, A. Ben-Cohen, G. Kaissis, A. Szeskin, C. Jacobs, G. E. H. Mamani, G. Chartrand *et al.*, "The liver tumor segmentation benchmark (lits)," *Medical Image Analysis*, vol. 84, p. 102680, 2023.
- [79] M. R. Hernandez Petzsche, E. de la Rosa, U. Hanning, R. Wiest, W. Valenzuela, M. Reyes, M. Meyer, S.-L. Liew, F. Kofler, I. Ezhov *et al.*, "Isles 2022: A multi-center magnetic resonance imaging stroke lesion segmentation dataset," *Scientific data*, vol. 9, no. 1, p. 762, 2022.
- [80] N. Shusharina and T. Bortfeld, "Glioma image segmentation for radiotherapy: Rt targets, barriers to cancer spread, and organs at risk (glis-rt)," *The Cancer Imaging Archive*, 2021. [Online]. Available: <https://doi.org/10.7937/TCIA.T905-ZQ20>
- [81] N. Shusharina, T. Bortfeld, C. Cardenas, B. De, K. Diao, S. Hernandez, Y. Liu, S. Maroongroge, J. Söderberg, and M. Soliman, "Cross-modality brain structures image segmentation for the radiotherapy target definition and plan optimization," in *Segmentation, Classification, and Registration of Multi-modality Medical Imaging Data: MICCAI 2020 Challenges, ABCs 2020, L2R 2020, TN-SCUI 2020, Held in Conjunction with MICCAI 2020, Lima, Peru, October 4–8, 2020, Proceedings 23*. Springer, 2021, pp. 3–15.
- [82] N. Shusharina, J. Söderberg, D. Edmunds, F. Löfman, H. Shih, and T. Bortfeld, "Automated delineation of the clinical target volume using anatomically constrained 3d expansion of the gross tumor volume," *Radiotherapy and Oncology*, vol. 146, pp. 37–43, 2020.
- [83] A. Jaus, C. Seibold, K. Hermann, A. Walter, K. Giske, J. Haubold, J. Kleesiek, and R. Stiefelhagen, "Towards unifying anatomy segmentation: Automated generation of a full-body ct dataset via knowledge aggregation and anatomical guidelines," *arXiv preprint arXiv:2307.13375*, 2023.
- [84] S. Gatidis, T. Hepp, M. Früh, C. La Fougère, K. Nikolaou, C. Pfannenberger, B. Schölkopf, T. Küstner, C. Cyran, and D. Rubin, "A whole-body fdg-pet/ct dataset with manually annotated tumor lesions," *Scientific Data*, vol. 9, no. 1, p. 601, 2022.
- [85] S. Gatidis, M. Früh, M. Fabritius, S. Gu, K. Nikolaou, C. La Fougère, J. Ye, J. He, Y. Peng, L. Bi, J. Ma, B. Wang, J. Zhang, Y. Huang, L. Heiliger, Z. Marinov, R. Stiefelhagen, J. Egger, J. Kleesiek, L. Sibille, L. Xiang, S. Bendazolli, M. Astaraki, B. Schölkopf, M. Ingrisch, C. Cyran, and T. Küstner, "The autopet challenge: Towards fully automated lesion segmentation in oncologic pet/ct imaging," *Research Square preprint doi.org/10.21203/rs.3.rs-2572595/v1*, 2023.
- [86] S. Gatidis and T. Küstner, "A whole-body fdg-pet/ct dataset with manually annotated tumor lesions," *The Cancer Imaging Archive*, 2022. [Online]. Available: <https://doi.org/10.7937/gkr0-xv29>
- [87] J. Ma, Y. Zhang, S. Gu, C. Zhu, C. Ge, Y. Zhang, X. An, C. Wang, Q. Wang, X. Liu, S. Cao, Q. Zhang, S. Liu, Y. Wang, Y. Li, J. He, and X. Yang, "Abdoment-1k: Is abdominal organ segmentation a solved problem?" *IEEE Transactions on Pattern Analysis and Machine Intelligence*, vol. 44, no. 10, pp. 6695–6714, 2022.
- [88] J. Ma, Y. Zhang, S. Gu, X. An, Z. Wang, C. Ge, C. Wang, F. Zhang, Y. Wang, Y. Xu *et al.*, "Fast and low-gpu-memory abdomen ct organ segmentation: the flare challenge," *Medical Image Analysis*, vol. 82, p. 102616, 2022.
- [89] A. L. Simpson, M. Antonelli, S. Bakas, M. Bilello, K. Farahani, B. Van Ginneken, A. Kopp-Schneider, B. A. Landman, G. Litjens, B. Menze *et al.*, "A large annotated medical image dataset for the development and evaluation of segmentation algorithms," *arXiv preprint arXiv:1902.09063*, 2019.
- [90] J. Ma, Y. Zhang, S. Gu, C. Ge, S. Ma, A. Young, C. Zhu, K. Meng, X. Yang, Z. Huang, F. Zhang, W. Liu, Y. Pan, S. Huang, J. Wang, M. Sun, W. Xu, D. Jia, J. W. Choi, N. Alves, B. de Wilde, G. Koehler, Y. Wu, M. Wiesenfarth, Q. Zhu, G. Dong, J. He, the FLARE Challenge Consortium, and B. Wang, "Unleashing the strengths of unlabeled data in pan-cancer abdominal organ quantification: the flare22 challenge," *arXiv preprint arXiv:2308.05862*, 2023.
- [91] M. Cipriano, S. Allegretti, F. Bolelli, F. Pollastri, and C. Grana, "Improving Segmentation of the Inferior Alveolar Nerve through Deep Label Propagation," in *IEEE/CVF Conference on Computer Vision and Pattern Recognition (CVPR)*. IEEE, Jun 2022, pp. 21 137–21 146.
- [92] F. Bolelli, L. Lumetti, M. Di Bartolomeo, S. Vinayahalingam, A. Anesi, B. van Ginneken, and C. Grana, "Tooth Fairy: A Cone-Beam Computed Tomography Segmentation Challenge," in *Structured Challenge*. Structured Challenge, Sep 2023.
- [93] R. Gharleghi, D. Adikari, K. Ellenberger, S.-Y. Ooi, C. Ellis, C.-M. Chen, R. Gao, Y. He, R. Hussain, C.-Y. Lee, J. Li, J. Ma, Z. Nie, B. Oliveira, Y. Qi, Y. Skandarani, J. L. Vilaça, X. Wang, S. Yang, A. Sowmya, and S. Beier, "Automated segmentation of normal and diseased coronary arteries – the asoca challenge," *Computerized Medical Imaging and Graphics*, vol. 97, p. 102049, 2022. [Online]. Available: <https://www.sciencedirect.com/science/article/pii/S0895611122000222>
- [94] R. Gharleghi, D. Adikari, K. Ellenberger, M. Webster, C. Ellis, A. Sowmya, S. Ooi, and S. Beier, "Annotated computed tomography coronary angiogram images and associated data of normal and diseased arteries," *Scientific Data*, vol. 10, no. 1, p. 128, 2023.
- [95] R. Souza, O. Lucena, J. Garrafa, D. Gobbi, M. Saluzzi, S. Appenzeller, L. Rittner, R. Frayne, and R. Lotufo, "An open, multi-vendor, multi-field-strength brain mr dataset and analysis of publicly available skull stripping methods agreement," *NeuroImage*, vol. 170, pp. 482–494, 2018.
- [96] D. Angeles-Valdez, J. Rasgado-Toledo, V. Issa-Garcia, T. Balducci, V. Villicaña, A. Valencia, J. J. Gonzalez-Olvera, E. Reyes-Zamorano, and E. A. Garza-Villarreal, "The mexican magnetic resonance imaging dataset of patients with cocaine use disorder: Sudmex conn," *Scientific data*, vol. 9, no. 1, p. 133, 2022.
- [97] Y. Ji, H. Bai, C. Ge, J. Yang, Y. Zhu, R. Zhang, Z. Li, L. Zhanng, W. Ma, X. Wan *et al.*, "Amos: A large-scale abdominal multi-organ benchmark for versatile medical image segmentation," *Advances in Neural Information Processing Systems*, vol. 35, pp. 36 722–36 732, 2022.
- [98] J. Pedrosa, G. Aresta, C. Ferreira, M. Rodrigues, P. Leitão, A. S. Carvalho, J. Rebelo, E. Negrão, I. Ramos, A. Cunha *et al.*, "Lndb: a lung nodule database on computed tomography," *arXiv preprint arXiv:1911.08434*, 2019.
- [99] J. Pedrosa, G. Aresta, C. Ferreira, G. Atwal, H. A. Phoulady, X. Chen, R. Chen, J. Li, L. Wang, A. Galdran *et al.*, "Lndb challenge on automatic lung cancer patient management," *Medical image analysis*, vol. 70, p. 102027, 2021.
- [100] G. Litjens, R. Toth, W. Van De Ven, C. Hoeks, S. Kerkstra, B. Van Ginneken, G. Vincent, G. Guillard, N. Birbeck, J. Zhang *et al.*, "Evaluation of prostate segmentation algorithms for mri: the promise12 challenge," *Medical image analysis*, vol. 18, no. 2, pp. 359–373, 2014.
- [101] A. Lalande, Z. Chen, T. Decourselle, A. Qayyum, T. Pommier, L. Lorgis, E. de La Rosa, A. Cochet, Y. Cottin, D. Ginjac *et al.*, "Emidec: a database usable for the automatic evaluation of myocardial infarction from delayed-enhancement cardiac mri," *Data*, vol. 5, no. 4, p. 89, 2020.
- [102] A. Lalande, Z. Chen, T. Pommier, T. Decourselle, A. Qayyum, M. Salomon, D. Ginjac, Y. Skandarani, A. Boucher, K. Brahim *et al.*, "Deep learning methods for automatic evaluation of delayed enhancement-mri: the results of the emidec challenge," *Medical Image Analysis*, vol. 79, p. 102428, 2022.
- [103] B. Rister, D. Yi, K. Shivakumar, T. Nobashi, and D. L. Rubin, "Ct-org, a new dataset for multiple organ segmentation in computed tomography," *Scientific Data*, vol. 7, no. 1, p. 381, 2020.

- [104] Y. Suter, U. Knecht, W. Valenzuela, M. Notter, E. Hewer, P. Schucht, R. Wiest, and M. Reyes, "The lumiere dataset: Longitudinal glioblastoma mri with expert rano evaluation," *Scientific data*, vol. 9, no. 1, p. 768, 2022.
- [105] W. E. Lorensen and H. E. Cline, "Marching cubes: A high resolution 3d surface construction algorithm," *ACM siggraph computer graphics*, vol. 21, no. 4, pp. 163–169, 1987.
- [106] M. Eisenmann, A. Reinke, V. Weru, M. D. Tizabi, F. Isensee, T. J. Adler, P. Godau, V. Cheplygina, M. Kozubek, S. Ali *et al.*, "Biomedical image analysis competitions: The state of current participation practice," *arXiv preprint arXiv:2212.08568*, 2022.
- [107] M. Eisenmann *et al.*, "Why is the winner the best?" in *Proceedings of The IEEE / CVF Computer Vision and Pattern Recognition Conference (CVPR)*, 2023.
- [108] M. Eisenmann, A. Reinke, V. Weru, M. D. Tizabi, F. Isensee, T. J. Adler, S. Ali, V. Andrearczyk, M. Aubreville, U. Baid *et al.*, "Why is the winner the best?" in *Proceedings of the IEEE/CVF Conference on Computer Vision and Pattern Recognition*, 2023, pp. 19955–19966.
- [109] J. W. de Kok, M. Á. A. de la Hoz, Y. de Jong, V. Brokke, P. W. Elbers, P. Thorax, A. Castillejo, T. Trenor, J. M. Castellano, A. E. Bronchalo *et al.*, "A guide to sharing open healthcare data under the general data protection regulation," *Scientific data*, vol. 10, no. 1, p. 404, 2023.
- [110] F. N. Wirth, T. Meurers, M. Johns, and F. Prasser, "Privacy-preserving data sharing infrastructures for medical research: systematization and comparison," *BMC Medical Informatics and Decision Making*, vol. 21, no. 1, pp. 1–13, 2021.
- [111] J. W. Gichoya, I. Banerjee, A. R. Bhimireddy, J. L. Burns, L. A. Celi, L.-C. Chen, R. Correa, N. Dullerud, M. Ghassemi, S.-C. Huang *et al.*, "Ai recognition of patient race in medical imaging: a modelling study," *The Lancet Digital Health*, vol. 4, no. 6, pp. e406–e414, 2022.
- [112] A. Sharma and G. Shrimal, "Ai-based medical image inspection for patient's racial identity recognition," in *2022 International Conference on Futuristic Technologies (INCOFT)*. IEEE, 2022, pp. 1–9.
- [113] C. G. Schwarz, W. K. Kremers, T. M. Therneau, R. R. Sharp, J. L. Gunter, P. Vemuri, A. Arani, A. J. Szychala, K. Kantarci, D. S. Knopman *et al.*, "Identification of anonymous mri research participants with face-recognition software," *New England Journal of Medicine*, vol. 381, no. 17, pp. 1684–1686, 2019.
- [114] F. Isensee, P. F. Jaeger, S. A. Kohl, J. Petersen, and K. H. Maier-Hein, "nnu-net: a self-configuring method for deep learning-based biomedical image segmentation," *Nature methods*, vol. 18, no. 2, pp. 203–211, 2021.
- [115] A. Sekuboyina, M. E. Hussein, A. Bayat, M. Löffler, H. Liebl, H. Li, G. Tetteh, J. Kukačka, C. Payer, D. Štern *et al.*, "Verse: A vertebrae labelling and segmentation benchmark for multi-detector ct images," *Medical image analysis*, vol. 73, p. 102166, 2021.
- [116] M. T. Löffler, A. Sekuboyina, A. Jacob, A.-L. Grau, A. Scharr, M. El Hussein, M. Kallweit, C. Zimmer, T. Baum, and J. S. Kirschke, "A vertebral segmentation dataset with fracture grading," *Radiology: Artificial Intelligence*, vol. 2, no. 4, p. e190138, 2020.
- [117] H. Liebl, D. Schinz, A. Sekuboyina, L. Malagutti, M. T. Löffler, A. Bayat, M. El Hussein, G. Tetteh, K. Grau, E. Niederreiter *et al.*, "A computed tomography vertebral segmentation dataset with anatomical variations and multi-vendor scanner data," *Scientific data*, vol. 8, no. 1, p. 284, 2021.
- [118] M. Cipriano, S. Allegretti, F. Bolelli, M. Di Bartolomeo, F. Pollastri, A. Pellacani, P. Minafra, A. Anesi, and C. Grana, "Deep Segmentation of the Mandibular Canal: a New 3D Annotated Dataset of CBCT Volumes," *IEEE Access*, vol. 10, pp. 11 500–11 510, 2022.
- [119] M. Di Bartolomeo, A. Pellacani, F. Bolelli, M. Cipriano, L. Lumetti, S. Negrello, S. Allegretti, P. Minafra, F. Pollastri, R. Nocini, G. Colletti, L. Chiarini, C. Grana, and A. Anesi, "Inferior Alveolar Canal Automatic Detection with Deep Learning CNNs on CBCTs: Development of a Novel Model and Release of Open-Source Dataset and Algorithm," *Applied Sciences*, vol. 13, no. 5, 2023.
- [120] L. Lumetti, V. Pipoli, F. Bolelli, and C. Grana, "Annotating the Inferior Alveolar Canal: the Ultimate Tool," in *Image Analysis and Processing - ICIAP 2023*. Springer, Oct 2023, pp. 1–12.
- [121] C. Mercadante, M. Cipriano, F. Bolelli, F. Pollastri, M. Di Bartolomeo, A. Anesi, and C. Grana, "A Cone Beam Computed Tomography Annotation Tool for Automatic Detection of the Inferior Alveolar Nerve Canal," in *Proceedings of the 16th International Joint Conference on Computer Vision, Imaging and Computer Graphics Theory and Applications - Volume 4: VISAPP*, vol. 4. SciTePress, Feb 2021, pp. 724–731.
- [122] C. Seibold, A. Jaus, M. A. Fink, M. Kim, S. Reiß, K. Herrmann, J. Kleesiek, and R. Stiefelhagen, "Accurate fine-grained segmentation of human anatomy in radiographs via volumetric pseudo-labeling," *arXiv preprint arXiv:2306.03934*, 2023.
- [123] C. M. Seibold, S. Reiß, J. Kleesiek, and R. Stiefelhagen, "Reference-guided pseudo-label generation for medical semantic segmentation," in *Proceedings of the AAAI conference on artificial intelligence*, vol. 36, no. 2, 2022, pp. 2171–2179.
- [124] B. B. Avants, N. J. Tustison, G. Song, P. A. Cook, A. Klein, and J. C. Gee, "A reproducible evaluation of ANTs similarity metric performance in brain image registration," *NeuroImage*, vol. 54, no. 3, pp. 2033–2044, 2011.
- [125] S. F. Eskildsen, P. Coupé, V. Fonov, J. V. Manjòn, K. K. Leung, N. Guizard, S. N. Wassef, L. R. Østergaard, and D. L. Collins, "BEAST: Brain extraction based on non-local segmentation technique," *NeuroImage*, vol. 59, no. 3, pp. 2362–2373, 2012.
- [126] S. M. Smith, "Fast robust automated brain extraction," *Human Brain Mapping*, vol. 17, no. 3, pp. 143–155, Nov. 2002.
- [127] D. W. Shattuck, S. R. Sandor-Leahy, K. A. Schaper, D. A. Rottenberg, and R. M. Leahy, "Magnetic resonance image tissue classification using a partial volume model," *NeuroImage*, vol. 13, no. 5, pp. 856–876, may 2001.
- [128] F. Ségonne, A. M. Dale, B. E. Busa, B. M. Glessner, B. D. Salat, B. H. K. Hahn, and B. F. A, "A hybrid approach to the skull stripping problem in MRI," *NeuroImage*, vol. 22, 2004.
- [129] R. Beare, J. Chen, C. Adamson, T. Silk, D. Thompson, J. Yang, V. Anderson, M. Seal, and A. Wood, "Brain extraction using the watershed transform from markers," *Frontiers in Neuroinformatics*, vol. 7, no. 32, December 2013.
- [130] E. S. Lutkenhoff, M. Rosenberg, J. Chiang, K. Zhang, J. D. Pickard, A. M. Owen, and M. M. Monti, "Optimized brain extraction for pathological brains (OPTIBET)," *PLoS ONE*, vol. 9, no. 12, pp. 1–13, 12 2014.
- [131] J. E. Iglesias, C. Y. Liu, P. M. Thompson, and Z. Tu, "Robust brain extraction across datasets and comparison with publicly available methods," *IEEE Transactions on Medical Imaging*, vol. 30, no. 9, pp. 1617–1634, Sept 2011.
- [132] S. K. Warfield, K. H. Zou, and W. M. Wells, "Simultaneous truth and performance level estimation (STAPLE): an algorithm for the validation of image segmentation," *IEEE Transactions on Medical Imaging*, vol. 23, no. 7, pp. 903–921, July 2004.
- [133] O. Lucena, R. Souza, L. Rittner, R. Frayne, and R. Lotufo, "Convolutional neural networks for skull-stripping in brain mr imaging using silver standard masks," *Artificial intelligence in medicine*, vol. 98, pp. 48–58, 2019.
- [134] S. Kaliyugarasan, M. Kocinski, A. Lundervold, and A. S. Lundervold, "2d and 3d u-nets for skull stripping in a large and heterogeneous set of head mri using fastai," 2020.
- [135] P. Saat, N. Nogovitsyn, M. Y. Hassan, M. A. Ganaie, R. Souza, and H. Hemmati, "A domain adaptation benchmark for t1-weighted brain magnetic resonance image segmentation," *Frontiers in Neuroinformatics*, p. 96, 2022.
- [136] B. Shirokikh, I. Zakazov, A. Chernyavskiy, I. Fedulova, and M. Belyaev, "First u-net layers contain more domain specific information than the last ones," in *Domain Adaptation and Representation Transfer, and Distributed and Collaborative Learning: Second MICCAI Workshop, DART 2020, and First MICCAI Workshop, DCL 2020, Held in Conjunction with MICCAI 2020, Lima, Peru, October 4–8, 2020, Proceedings 2*. Springer, 2020, pp. 117–126.
- [137] G. Yiasemis, J.-J. Sonke, C. Sánchez, and J. Teuwen, "Recurrent variational network: a deep learning inverse problem solver applied to the task of accelerated mri reconstruction," in *Proceedings of the IEEE/CVF conference on computer vision and pattern recognition*, 2022, pp. 732–741.
- [138] J. Beauferris, J. Teuwen, D. Karkalousos, N. Moriakov, M. Caan, G. Yiasemis, L. Rodrigues, A. Lopes, H. Pedrini, L. Rittner *et al.*, "Multi-coil mri reconstruction challenge—assessing brain mri reconstruction models and their generalizability to varying coil configurations," *Frontiers in Neuroscience*, vol. 16, p. 919186, 2022.

- [139] Ö. Çiçek, A. Abdulkadir, S. S. Lienkamp, T. Brox, and O. Ronneberger, "3d u-net: learning dense volumetric segmentation from sparse annotation," in *Medical Image Computing and Computer-Assisted Intervention—MICCAI 2016: 19th International Conference, Athens, Greece, October 17-21, 2016, Proceedings, Part II 19*. Springer, 2016, pp. 424–432.
- [140] A. Ferreira, J. Li, K. L. Pomykala, J. Kleesiek, V. Alves, and J. Egger, "Gan-based generation of realistic 3d data: A systematic review and taxonomy," *arXiv preprint arXiv:2207.01390*, 2022.
- [141] J. Yu, H. Zhu, L. Jiang, C. C. Loy, W. Cai, and W. Wu, "Celebv-text: A large-scale facial text-video dataset," in *Proceedings of the IEEE/CVF Conference on Computer Vision and Pattern Recognition (CVPR)*, June 2023, pp. 14 805–14 814.
- [142] J. Xing, M. Xia, Y. Zhang, X. Cun, J. Wang, and T.-T. Wong, "Codetalker: Speech-driven 3d facial animation with discrete motion prior," in *Proceedings of the IEEE/CVF Conference on Computer Vision and Pattern Recognition (CVPR)*, June 2023, pp. 12 780–12 790.
- [143] G. Fanelli, J. Gall, H. Romsdorfer, T. Weise, and L. Van Gool, "A 3-d audio-visual corpus of affective communication," *IEEE Transactions on Multimedia*, vol. 12, no. 6, pp. 591–598, 2010.
- [144] D. Cudeiro, T. Bolkart, C. Laidlaw, A. Ranjan, and M. J. Black, "Capture, learning, and synthesis of 3d speaking styles," in *Proceedings of the IEEE/CVF Conference on Computer Vision and Pattern Recognition*, 2019, pp. 10 101–10 111.
- [145] S. Missal, "Forensic facial reconstruction of skeletonized and highly decomposed human remains," in *Forensic Genetic Approaches for Identification of Human Skeletal Remains*. Elsevier, 2023, pp. 549–569.
- [146] M. D. Klarqvist, S. Agrawal, N. Diamant, P. T. Ellinor, A. Philippakis, K. Ng, P. Batra, and A. V. Khera, "Silhouette images enable estimation of body fat distribution and associated cardiometabolic risk," *NPJ Digital Medicine*, vol. 5, no. 1, p. 105, 2022.
- [147] B. Sauty and S. Durrleman, "Progression models for imaging data with longitudinal variational auto encoders," in *International Conference on Medical Image Computing and Computer-Assisted Intervention*. Springer, 2022, pp. 3–13.
- [148] D. P. Kingma and M. Welling, "Auto-encoding variational bayes," *arXiv preprint arXiv:1312.6114*, 2013.
- [149] J. Li, A. Pepe, G. Luijten, C. Schwarz-Gsaxner, and J. Kleesiek, "Anatomy completer: A multi-class completion framework for 3d anatomy reconstruction," *arXiv preprint*, 2023.
- [150] D. Anguelov, P. Srinivasan, D. Koller, S. Thrun, J. Rodgers, and J. Davis, "Scape: shape completion and animation of people," in *ACM SIGGRAPH 2005 Papers*, 2005, pp. 408–416.
- [151] Y.-C. Cheng, H.-Y. Lee, S. Tulyakov, A. G. Schwing, and L.-Y. Gui, "Sdfusion: Multimodal 3d shape completion, reconstruction, and generation," in *Proceedings of the IEEE/CVF Conference on Computer Vision and Pattern Recognition*, 2023, pp. 4456–4465.
- [152] W. Yuan, T. Khot, D. Held, C. Mertz, and M. Hebert, "Pcn: Point completion network," in *2018 International Conference on 3D Vision (3DV)*. IEEE, 2018, pp. 728–737.
- [153] B. Gong, Y. Nie, Y. Lin, X. Han, and Y. Yu, "Me-pcn: Point completion conditioned on mask emptiness," in *Proceedings of the IEEE/CVF international conference on computer vision*, 2021, pp. 12 488–12 497.
- [154] X. Yu, Y. Rao, Z. Wang, Z. Liu, J. Lu, and J. Zhou, "Pointnet: Diverse point cloud completion with geometry-aware transformers," in *Proceedings of the IEEE/CVF international conference on computer vision*, 2021, pp. 12 498–12 507.
- [155] J. Li, J. Fragemann, S.-A. Ahmadi, J. Kleesiek, and J. Egger, "Training  $\beta$ -vae by aggregating a learned gaussian posterior with a decoupled decoder," in *MICCAI Workshop on Medical Applications with Disentanglements*. Springer, 2022, pp. 70–92.
- [156] K. Sharma, A. Kaur, and S. Gujral, "Brain tumor detection based on machine learning algorithms," *International Journal of Computer Applications*, vol. 103, no. 1, 2014.
- [157] J. Amin, M. Sharif, M. Raza, T. Saba, and M. A. Anjum, "Brain tumor detection using statistical and machine learning method," *Computer methods and programs in biomedicine*, vol. 177, pp. 69–79, 2019.
- [158] J. Amin, M. Sharif, A. Haldorai, M. Yasmin, and R. S. Nayak, "Brain tumor detection and classification using machine learning: a comprehensive survey," *Complex & intelligent systems*, pp. 1–23, 2021.
- [159] J. Kleesiek, G. Urban, A. Hubert, D. Schwarz, K. Maier-Hein, M. Bendszus, and A. Biller, "Deep mri brain extraction: A 3d convolutional neural network for skull stripping," *NeuroImage*, vol. 129, pp. 460–469, 2016.
- [160] C. Gsaxner, J. Li, A. Pepe, Y. Jin, J. Kleesiek, D. Schmalstieg, and J. Egger, "The hololens in medicine: A systematic review and taxonomy," *Medical Image Analysis*, p. 102757, 2023.
- [161] K. A. Bölek, G. De Jong, and D. Henssen, "The effectiveness of the use of augmented reality in anatomy education: a systematic review and meta-analysis," *Scientific Reports*, vol. 11, no. 1, p. 15292, 2021.
- [162] A. S. Jwa and R. A. Poldrack, "The spectrum of data sharing policies in neuroimaging data repositories," *Human Brain Mapping*, vol. 43, no. 8, pp. 2707–2721, 2022.
- [163] N. Khalid, A. Qayyum, M. Bilal, A. Al-Fuqaha, and J. Qadir, "Privacy-preserving artificial intelligence in healthcare: Techniques and applications," *Computers in Biology and Medicine*, p. 106848, 2023.
- [164] F. Gießler, M. Thormann, B. Preim, D. Behme, and S. Saalfeld, "Facial feature removal for anonymization of neurological image data," in *Current Directions in Biomedical Engineering*, vol. 7, no. 1. De Gruyter, 2021, pp. 130–134.
- [165] A. E. Theyers, M. Zamyadi, M. O'Reilly, R. Bartha, S. Symons, G. M. MacQueen, S. Hassel, J. P. Lerch, E. Anagnostou, R. W. Lam *et al.*, "Multisite comparison of mri defacing software across multiple cohorts," *Frontiers in psychiatry*, vol. 12, p. 617997, 2021.